Reconstructing hydroclimate changes of past 2,500 years using speleothems from Pyrenean caves (NE Spain)

Miguel Bartolomé[1,2,3*], Ana Moreno[4*], Carlos Sancho[5†], Isabel Cacho[6], Heather Stoll[3], Negar Haghipour[3,7], Ánchel Belmonte[8], Christoph Spötl[9], John Hellstrom[10], R. Lawrence Edwards[11] and Hai Cheng[12,13,14]

[1] Departamento de Geología. Museo Nacional de Ciencias Naturales (CSIC). C. de José Gutiérrez Abascal, 2, 28006 Madrid, Spain.

[2] Swiss Institute for Speleology and Karst Studies (SISKA), Rue de la Serre 68 2300 La Chaux-de-Fonds, Switzerland.

[3] Geological Institute, NO G59, Department of Earth Sciences, Sonneggstrasse 5, ETH, 8092 Zurich, Switzerland.

[4] Department of Geoenvironmental Processes and Global Change, Pyrenean Institute of Ecology (IPE-CSIC), Avda. Montañana 1005, 50059 Zaragoza, Spain.

[5†] Earth Sciences Department, University of Zaragoza, C/Pedro Cerbuna 12, 50009 Zaragoza, Spain. Deceased.

[6] CRG Geociències Marines, Dept. Dinàmica de la Terra i de l'Oceà, Universitat de Barcelona, 08028 Barcelona, Spain

[7] Laboratory for Ion Beam Physics, Department of Physics, ETH Zurich, Switzerland

[8] Sobrarbe-Pirineos UNESCO Global Geopark. Boltaña. Spain.

[9] Institute of Geology, University of Innsbruck, 6020, Innsbruck, Austria

[10] School of Earth Sciences, The University of Melbourne, VIC 3010, Australia

[11] Department of Earth and Environmental Sciences, University of Minnesota, Minneapolis, MN, 55455, USA

[12] Institute of Global Environmental Change, Xi'an Jiaotong University, Xi'an, 710049, China.

[13] State Key Laboratory of Loess and Quaternary Geology, Institute of Earth Environment, 11 Chinese Academy of Sciences, Xi'an, 710061, China.

[14] Key Laboratory of Karst Dynamics, MLR, Institute of Karst Geology, CAGS, Guilin, 541004, China.

* Both authors have contributed equally to this manuscript

Corresponding author: Ana Moreno (amoreno@ipe.csic.es)

Abstract. Reconstructing of past hydroclimates at regional scales during the Common Era (CE) is necessary to place the current warming in the context of natural climate variability. Here we present a composite record of oxygen isotope variations during last 2500 years based on eight stalagmites from four caves in the central Pyrenees (NE Spain) dominated by temperature variations, with amount of precipitation playing a minor role. The dataset is compared with other Iberian reconstructions that show a high degree of internal coherence with respect to variability at the centennial scale. The Roman Period (RP) (especially 0-200 CE), the Medieval Climate Anomaly (MCA), and part of the Little Ice Age (LIA) represent the warmest periods, while the coldest decades occurred during the Dark Ages (DA) and most of the LIA intervals (e.g., 520-550 CE and 1800-1850 CE). Importantly, the LIA cooling or the MCA warming were not continuous or uniform and exhibited high decadal variability. The Industrial Era (IE) shows an overall warming trend although with marked cycles and partial stabilization during the last two decades (1990-2010). The strong coherence between the speleothem data, European temperature reconstructions and global tree-ring data informs about the regional representativeness of this new record as Pyrenean past climate variations. Solar variability, likely through its impact on the North Atlantic Oscillation, and major volcanic eruptions appear to be the two main drivers of climate in southwestern Europe during the past 2.5 millennia.

Keywords. Iberian Peninsula, Central Pyrenees, late Holocene, stalagmite, temperature reconstruction

1. Introduction

Global surface temperatures in the first two decades of the 21st century (2001–2020) were 0.84 to 1.10 °C warmer than 1850–1900 CE (IPCC, 2021). There is strong evidence that anthropogenic global warming is unprecedented in terms of absolute temperatures and spatial consistency over the past 2000 yr (Ahmed et al., 2013; Konecky et al., 2020). On the contrary, pre-industrial temperatures were less spatially coherent, and further work is needed to explain the regional expression of climate change (Mann, 2021; Neukom et al., 2019). Obtaining new and high-quality records in terms of resolution, dating and regional representativeness is thus critical for characterizing natural climate variability on decadal to centennial scales (PAGES2k Consortium et al., 2017).

High mountains are particularly sensitive regions to climate change and among them the Pyrenees occupy a crucial frontier position in southern Europe, influenced by both Mediterranean and Atlantic climates. In the Pyrenees, the temperature has increased by more than 1.5°C since 1882, as shown by the longest time series from the Pic du Midi observatory (Bücher and Dessens, 1991; Dessens and Bücher, 1995). Recent studies confirm this warming trend, showing an increase of 0.1 °C per decade during the last century in Central Pyrenees (Pérez-Zanón et al., 2017), or even 0.28°C per decade if only the 1959-2015 period is considered (Observatorio Pirenaico de Cambio Global, 2018). Long-term snow depth observations (starting in 1955) show a statistically significant decline, especially at elevations above 2000 m a.s.l. (López-Moreno et al., 2020). This fact, together with the increase in temperature, has caused the glaciated area in the Pyrenees to decrease by 21.9% in the last decade (Vidaller et al., 2021), changing from 2060 ha during the LIA to 242 ha in 2016 (Rico et al., 2017). Recent studies on one of the emblematic glaciers in the Pyrenees, the Monte Perdido glacier, show that the current ice retreat is unprecedent in the last 2000 years, as this glacier survived previous warm periods such as the MCA and the RP (Moreno et al., 2021b).

The study of sediment records from lakes in the Pyrenees, where considerable variations in water level, water chemistry, and biological processes have occurred due to changes in effective moisture and temperature, is an excellent approach to reconstruct past climate variability (González-Sampériz et al., 2017). Recently, a comprehensive study in six high altitude Pyrenean lakes indicates unprecedented changes in the lithogenic and organic carbon fluxes since 1950 CE, suggesting an increase in algal productivity likely favoured by warmer temperatures and higher nutrient deposition associated to the Great Acceleration (Vicente de Vera García et al., 2023), a period when human-driven global, social, technological, and environmental changes intensifying dramatically (Steffen et al., 2015). Marine records off the Iberian coast show a clear long-term cooling trend, from 0 CE to the beginning of the 20th century, probably reflecting the decline in Northern Hemisphere summer insolation that began after the Holocene optimum (Abrantes et al., 2017). Unfortunately, it is not possible to record decadal temperature changes from the studied proxies of these lake or marine records, so other archives allowing higher chronological robustness and larger resolution are required.

The Central Pyrenees are largely composed of limestones and host numerous caves, some of which are rich in speleothems, thus making it possible to reconstruct the past climate by studying stalagmites from different caves. Unfortunately, despite the high potential of stalagmite with annually to sub-annual resolution in the CE, it is extremely difficult to obtain high-resolution and well-replicated records. In most cases, the CE period spans only a few centimetres, limiting the number of samples drilled for high-precision U-Th dating (PAGES Hydro2k Consortium, 2017). In addition to this chronological challenge, the interpretation of oxygen isotopes of speleothems ($\delta^{18}O_c$) from southern Europe is also complex (Moreno et al., 2021a). Recent studies of Pyrenean stalagmites covering the last deglaciation indicate the important role of changes in annual temperature in the variability of $\delta^{18}O_c$ (Bartolomé et al., 2015a; Bernal-Wormull et al., 2021). However, correct interpretation of $\delta^{18}O_c$ proxies requires a sound understanding of the influence of climate variables on carbonate deposition in caves through monitoring (e.g. Pérez-Mejías et al., 2018) and calibration to the instrumental period (Mangini et al., 2005; Tadros et al., 2022).

In this study, we provide high-resolution $\delta^{18}O_c$ data for eight stalagmites from four different caves in the Central Pyrenees, allowing us to construct a stacked curve of climate variability for the last 2500 years with

98   potential regional representativeness. These eight stalagmites allow climate changes during the CE to be
99   studied in reasonably robust chronological framework. Monitoring and calibration of $\delta^{18}O_c$ with
100   instrumental data for the two youngest stalagmites suggests that the $\delta^{18}O_c$ variability primarily reflects
101   annual temperatures, while precipitation (eg. amount of precipitation, seasonality, source) played a role
102   during certain periods. This new record represents an excellent opportunity to characterize natural
103   temperature changes in this region on decadal to centennial scales for the last 2500 years and compare them
104   with other approaches to examine their regional representativeness.

105   **2. Study sites**

106   **2.1. Geological setting, climate and vegetation**

107   This study of speleothems is located in the central sector of the Pyrenees, in northeastern Iberia (Fig. 1a,b).
108   All caves are located in the Sobrarbe Geopark, close to or at the borders of the Ordesa and Monte Perdido
109   National Park, formed in Mesozoic and Cenozoic limestones and at different altitudes (Fig. 1c). This area
110   has a steep topography due to the high altitudinal gradient and constitutes the largest limestone massif in
111   Europe (with 22 peaks above 3000 m a.s.l.).

112   The climate is Mediterranean according to the Köppen classification. However, the high relief influences
113   the climate of this high-altitude area which is accurately described as humid sub-Mediterranean because of
114   higher rainfall than the typically Mediterranean climate, particularly for the caves above 1000 m a.s.l. where
115   annual precipitation is above 1000-1200mm and falls mostly as snow. In lower altitude caves (e.g. Seso
116   Cave) mean annual precipitation is 900 mm, concentrated in spring and fall. Mean air temperatures range
117   from 0.5 to 15°C, depending on the altitude.

118   Around the caves, in the valleys, there are mid-mountain forests dominated by *Pinus sylvestris* and *Quercus*
119   *ilex*, as well as shrublands, whereas the highlands are characterized by exposed rock with sparse vegetation
120   such as meadows.

121   **2.2. Cave locations**

122   Seso cave (42°27´23.08´´N; 0°02´23.18´´E, 794 m a.s.l.) is formed in the eastern flank of the Boltaña
123   Anticline, close to Boltaña village. The cave developed in unsoluble marly strata between limestone beds
124   of Eocene age. The cave system consists of two longitudinal shallow galleries (2-3m of limestone thickness
125   over the cave) controlled by the bedding and the main set of joints. Formation of this shallow cave involved
126   the mechanical removal of large amounts of marl under vadose conditions which took place about 60-40
127   ka BP (Bartolomé et al., 2015b). Subsequently, calcite speleothems formed which became more abundant
128   during the Holocene. Average annual temperature inside Seso cave is ~11.8ºC.

129   Las Gloces cave (42°35'40" N, 0°1'41´´W, 1243 m a.s.l.) is located on the border of the Ordesa National
130   Park, next to Fanlo village. The cave formed in limestones of Early Eocene age. The limestone´s thickness
131   above the cave is ~20-30 m. Two galleries form the cave. The upper one preserves phreatic features and
132   hosts the majority of speleothems located in a small room, while vadose morphologies characterize the
133   lower gallery. Average annual temperature where the stalagmites were taken is ~ 9.8 ºC

134   B-1 cave (42°36'0.2''N; 0°7'46''E; 1090 m a.s.l.) is the lower entrance of the Las Fuentes de Escuaín
135   karstic system, and acts as the collector of all water drained by the system. This system comprises more
136   than 40 km of galleries and shows a vertical extension of -1150 m. It drains an area of ~15 km^2 and
137   developed mostly in Eocene limestones. Since a river runs through the cave, several detrital sequences
138   appear, as well as speleothems, affected by floods. The cave is then well ventilated and shows annual
139   temperature variations in response to the seasonal ventilation changes and seasonal flooding. The studied
140   sample was obtained in a fossil gallery, not currently influenced by flooding and with an average annual
141   temperature of ~9.5ºC.

142 Pot au Feu cave (42°31.48' N; 0°14.26' W; 996 m a.s.l.) is located in the Irués river valley in the Cotiella
143 massif. The host rock is an Upper Cretaceous limestone. Hydrogeologically, the cave belongs to the high
144 mountain unconfined karst Cotiella-Turbón aquifer but located in a non-active level. The cave comprises
145 horizontal galleries and small rooms connected by shafts formed by phreatic circulation. Some rooms are
146 well-decorated by large speleothems. The limestone thickness over the gallery where the stalagmite was
147 collected is approximately 800 m.

2.3. Cave climate

149 Understanding the modern microclimatic and hydrological conditions of caves is import for a sound
150 interpretation of speleothem proxy data (Genty et al., 2014; Lachniet, 2009; Moreno et al., 2014).
151 Particularly, the transfer of the stable isotopic signal from the rainfall to the dripwater and, eventually, to
152 the studied stalagmite is influenced by different processes in the atmosphere, soil and epikarst. Our
153 preliminary results for the Pyrenees show a seasonal pattern of precipitation isotopes consistent with the
154 annual temperature cycle (Moreno et al., 2021b). These data also suggest an interannual temperature−δ^{18}O
155 relationship of 0.47‰/°C (Giménez et al., 2021) that is only partially compensated by the -0.18 ‰/°C due
156 to the water-calcite isotope fractionation (Tremaine et al., 2011) thus allowing to use δ^{18}O in speleothems
157 as a temperature indicator in this region (see also Bartolomé et al., 2015a; Bernal-Wormull et al., 2021).

158 From the four studied caves, the best monitored one is Seso cave where a detailed monitoring survey was
159 conducted including analyses of δ^{18}O variability in rainfall, soil water, dripwater and farmed calcite
160 (Bartolomé, 2016). Seso cave developed under just few metres of rock, while the other caves are much
161 deeper, allowing a faster response to rainfall variability in Seso dripwaters and speleothems. Monitoring
162 carried out in Seso cave indicates a relationship between temperature and δ^{18}O of rainfall observed at
163 seasonal scale while rainfall isotopic composition is slightly modulated by the amount of precipitation
164 (Bartolomé et al., 2015a).

3. Methods

3.1. Speleothem samples

167 This study is based on eight stalagmites from four different caves in Central Pyrenees (Fig. 1c, Table 1).
168 The specimens were cut parallel to the growth axis and the central segment was sampled for U-Th dating,
169 stable isotopes (δ^{18}O and δ^{13}C) and Mg/Ca. Furthermore, the ^{14}C-activity of multiple samples from the top
170 of stalagmites MIC and XEV (both from Seso cave and underneath active drips) was determined in order
171 to detect the atmospheric bomb peak induced by the nuclear tests in 1945-1963.

172 Four small stalagmites were obtained from Seso cave, all showing fine laminations consisting of pairs of
173 dark-compact and light-porous laminae, but difficult to count due to their irregular pattern. The four Seso
174 stalagmites show medium to high porosity in some intervals, usually more frequent towards the top. MIC
175 (8.5 cm long) and XEV (26 cm long, composed of two stacked stalagmites – Appendix Fig. A1.a) were
176 sampled from base to top. In stalagmites CHA (8.5 cm long) and in CLA (10.5 cm long), the uppermost
177 interval was discarded due to the poor chronological control and associated to a possible hiatus above a
178 macroscopic discontinuity (Fig. A1.a).

179 Stalagmites ISA (13.5 cm long, with a visual hiatus at 7 cm above the base) and LUC (23.3 cm long, also
180 with a hiatus at 12.5 cm above the base) were sampled in Las Gloces cave (Fig. A1.b). Both are candle-
181 shaped with a slight tilt in the growth axis above their respective hiatus. One stalagmite, TAR, was obtained
182 from B1 cave which is an overgrowth over an older stalagmite composed of 7.5 cm of white carbonate that
183 is slightly laminated towards the top (Fig. A1.c). Finally, a 80 cm-long stalagmite (JAR) was obtained from
184 Pot au Feu cave. It is candle-shaped, laminated and lacks macroscopic hiatuses (Fig. A1.d).

3.2. Stable isotope and Mg/Ca analyses

186 Samples for stable isotopic ($\delta^{18}O$ and $\delta^{13}C$) analyses were microdrilled at 1-mm resolution along the growth
187 axis of seven of the eight speleothems (JAR from Pot au Feu was sampled every 5 mm) using a 0.5 mm
188 tungsten carbide dental bur. The first batch of the isotopic analyses was analysed at the University of
189 Barcelona (Scientific-Technical Services), Spain, using a Finnigan-MAT 252 mass spectrometer, linked to
190 a Kiel Carbonate Device III, with a reproducibility of 0.02‰ for $\delta^{13}C$ and 0.06‰ for $\delta^{18}O$. Calibration to
191 Vienna Pee Dee Belemnite (VPDB) was carried out by means of the NBS-19 standard. A second batch was
192 analysed at the University of Innsbruck using a ThermoFisher Delta V Plus isotope ratio mass spectrometer
193 coupled to a ThermoFisher GasBench II. Calibration of the instrument was accomplished using
194 international reference materials and the results are also reported relative to VPDB. Long-term precision
195 on the 1-sigma level is 0.06‰ and 0.08‰ for $\delta^{13}C$ and $\delta^{18}O$, respectively (Spötl, 2011).

196 The elemental chemical composition was analysed in the eight stalagmites (every 1 mm in Las Gloces,
197 Seso and B1 stalagmites and every 5 mm in JAR from Pot au Feu cave) using matrix-matched standards on
198 an inductively coupled plasma-atomic emission spectrometer (Thermo ICAP DUO 6300 at the Pyrenean
199 Institute of Ecology) following the procedure described in Moreno et al. (2010). Reported ratios are from
200 measurement of Ca (315.8 nm) and Mg (279.5 nm), all in radial mode.

201 3.3. U-Th dating and ^{14}C bomb peak

202 A total of 55 samples were prepared for U-Th dating, according to the U and Th chemical procedures
203 described in Edwards et al. (1987). Sample portions characterized by high porosity and voids were avoided
204 to minimize the effect of open system behaviour and possible age inversions. From those 55 samples, 45
205 were measured at the University of Minnesota (USA) and at the Xian' Jiaotong University (China) while
206 10 samples were analysed at the University of Melbourne (Australia) (samples of JAR) using the
207 methodology described in Hellstrom (2006). In the three laboratories, measurements were performed using
208 a MC-ICP-MS (Thermo-Finnigan Neptune or Nu Instruments) following previously described methods
209 (Cheng et al., 2013).

210 Due to the low U content (Table 2), the U-Th ages are not precise enough to obtain an accurate chronology
211 for the recent speleothem growth (see large errors in top samples in Fig. A1). Therefore, the ^{14}C "bomb
212 peak" method was applied to the MIC and XEV stalagmites that were actively growing in Seso cave at the
213 time of collection (2010 and 2013, respectively), confirmed by U/Th ages, albeit of low precision. We
214 drilled 10 and 8 subsamples for MIC and XEV, respectively (Fig. 2a and b), and ^{14}C activities were
215 measured using a novel online sampling and analysis method combining laser ablation with accelerator
216 mass spectrometry (LA-AMS) at the ETH Zurich (Welte et al., 2016). LA-AMS allows to produce spatially
217 resolved ^{14}C profiles of carbonate minerals with a precision of 1% for modern samples. The background
218 measured on ^{14}C-free marble ($F^{14}C = 0.011 \pm 0.002$) is low and reference carbonate material is well
219 reproduced. This method relies on the exploitation of the global anthropogenic increase in atmospheric ^{14}C
220 resulting from nuclear testing predominately in the 1950s and 1960s CE as a chronological marker in the
221 mid to late 20th Century (e.g., Genty et al., 1998; Hua et al., 2012). Atmospheric ^{14}C concentrations began
222 to rise in 1955 CE, peaking in the Northern Hemisphere (NH) in 1963 CE (Reimer, 2004). Because 80 to
223 90% of the carbon found in most speleothems comes from soil CO_2, this being linked to atmosphere CO_2,
224 it is likely that speleothem ^{14}C activity is close to the atmospheric ^{14}C activity or at least to the soil activity
225 (Markowska et al., 2019). Thus, the point where the ^{14}C concentration begins to rise, the highest
226 concentration point, and the date when the speleothem was removed from the cave (if actively dripping)
227 were used as chronological anchor points (Fig. 2a and b).

228 3.4. Age model

229 Age models were produced using StalAge software (Scholz and Hoffmann, 2011) for the eight speleothems
230 (Fig. A1) using the U-Th dates presented in Table 2. In the ISA stalagmite, one date was discarded due to
231 the large error (indicated in red in Table 2). During several intervals, two or more stalagmites grew
232 contemporaneously, allowing to test the reproducibility of the proxy records. We made the a priori
233 assumption that the $\delta^{18}O$ data of the selected stalagmites record a common rainfall and temperature signal,

234 given that these caves were only 20 km apart (Fig.1c). Then, the records are combined with *Iscam*
235 (Fohlmeister, 2012), a method that correlates dated proxy signals from several stalagmites, determines the
236 most probable age-depth model, and calculates the age uncertainty for the combined record.

237 In order to minimize the effect of different absolute isotopic values and ranges of individual stalagmite data
238 series, we detrended and normalized the δ^{18}O series using *Iscam*. Doing so, the interpretation of absolute
239 values will be precluded. Regarding the other parameters that can be changed in *Iscam*, we used point-wise
240 linear interpolation, 1000 Monte Carlo simulations and the smoothing window was fixed at 10 years. The
241 stalagmites were included in the *Iscam* composite record from the oldest to the youngest one as was the
242 order that provided the highest correlation coefficients: JAR- LUC – ISA -TAR – CHA – CLA -XEV and
243 MIC. The ISA sample was treated as two parts (ISA top and ISA base) to account for the hiatus, while LUC
244 was regarded as only one as StalAge does not suggest a hiatus in this stalagmite (Fig. A1.b). For the two
245 stalagmites that were active when collected, MIC and XEV, we also produced a composite record for the
246 last 200 years using *Iscam* (Fig. 2c). The use of Iscam software minimized the age uncertainty being lower
247 than the error in the U-Th dates. As an example, for last 600 years, the uncertainty is below 20 years.
248 However, it may reach 100 years for some particular intervals (eg. the century 1350-1250 AD).

249 In order to explore correlations among stalagmites from the same caves, we repeated the procedure to obtain
250 a composite record for the four stalagmites from Seso cave (CHA, CLA, XEV and MIC) (Fig. A2) and the
251 two from Las Gloces cave (ISA and LUC) (Fig. A3). In those two cases, we did not detrend or normalize
252 the individual records since they belong to the same cave and show the same range of δ^{18}O values. These
253 four records (composite records from Las Gloces and Seso caves, and individual stalagmites from Pot au
254 Feu and B1 caves) are show in Fig. 3 and compared to the final composite record. The composite δ^{18}O
255 record is used in this article as a proxy record for the Central Pyrenees climate of last 2500 years. We have
256 used approximate onset and end of five time subperiods, following previous literature (eg. Sánchez-López
257 et al., 2016): the end of the RP at 450 CE; DA (450-850 CE), MCA (850-1250 CE), LIA (1250-1950 CE)
258 and IE (since 1850 CE).

3.5. Statistical analyses

260 Statistical analyses were carried out using PAST software (Hammer et al., 2001). The δ^{18}O series and the
261 instrumental climatic series were first resampled (linear interpolation) to obtain the same regular spacing
262 (annual). Then, correlation was computed using Spearman's rank correlation analysis, a nonparametric
263 measure as an alternative to Pearson correlation analysis. This analysis was preferred to account for
264 nonlinear relationships, with r indicating the correlation coefficient and p-value, the probability value of
265 that correlation. The Bonferroni test was applied to prevent data from spuriously appearing as statistically
266 significant by making an adjustment during comparison testing (PAST software; Hammer et al, 2001).

267

4. Results

4.1. Age models and composite record

4.1.1. Detection of the bomb peak and composite record of the last 200 years

271 Stalagmites MIC and XEV from Seso cave were actively dripping when removed from the cave (in 2010
272 and 2013, respectively). Calcite deposited on glass plates placed below the two dripping points and
273 collected seasonally until 2021 demonstrates that the drip water is supersaturated with respect to calcite and
274 suggests that the top layer of both stalagmites was formed during the respective collection year (Fig. 2).
275 Therefore, these two stalagmites were analysed for their ^{14}C activity to identify the "bomb peak" and
276 improve the age model.

277 A strong increase in the ^{14}C activity is registered in the MIC and XEV stalagmites at 16 mm and 40 mm
278 depth from top (dft), respectively (Fig. 2a and b) with a rise in the fraction modern F^{14}C, interpreted as the

279 start of the mid-20th century atmospheric bomb peak. This allows defining the year 1955 CE, within ±2yr
280 uncertainties, at 16 mm dft in MIC and 40 mm dft in XEV (Fig. 2). All radiocarbon bomb peaks published
281 from speleothems show that the response of speleothem ^{14}C activity to the increase in atmospheric
282 radiocarbon activity occurred nearly simultaneously. However, whether the ^{14}C activity peak in a
283 speleothem can be assigned to the year 1963 CE depends on the soil properties and the thickness of the
284 rock above the cave, as well as the delay in the transfer of the atmospheric ^{14}C signal to the speleothem
285 (Fohlmeister et al., 2011; Hua et al., 2017). In the case of Seso cave, which is just 2-3 m below the surface
286 and the soils are patchy and thin (Bartolomé, 2016), the transfer of the ^{14}C signal was likely fast. We
287 therefore place the year 1963 CE, within ±2yr uncertainties, at 11 mm dft in MIC and at 25 mm dft in XEV
288 (Fig. 2a and b).

289 Since the two stalagmites MIC and XEV are the only ones in this study whose records extend to modern
290 times, we compare them with the instrumental record in order to improve the interpretation of the stable
291 isotope data. Thus, MIC and XEV δ^{18}O data were first combined using *Iscam* (Fig. 2c). Using the
292 parameters indicated in Methods (section 3.3), but without normalizing the records (both stalagmites belong
293 to the same cave and show the same range of δ^{18}O values) the correlation of stalagmites MIC and XEV
294 provided by *Iscam* software (r) is 0.81 (95% significance). This composite δ^{18}O record covers the last 200
295 years and has an amplitude of 0.9 ‰. The main feature (Fig. 2c) is a trend towards less negative values
296 (indicated by a polynomial line in Fig. 2c).

4.1.2. StalAge models and Iscam stack

298 Age models obtained by StalAge for individual stalagmites indicate that the growth rate was quite stable,
299 except of ISA and LUC, both from Las Gloces cave, where the growth rate changed after hiatuses (Fig.
300 A1.B). The temporal resolution of the stable isotope data allows to explore changes occurring on a decadal
301 scale (Table 1).

302 Using the parameters for constructing a composite record using *Iscam* (see Methods), correlation (r) value
303 (95% significance) of stalagmite JAR and LUC is 0.48, 0.67 between ISA_base and the combined stack of
304 JAR-LUC, 0.65 between ISA_top and the previous stack, 0.74 between TAR and the previous stack, 0.79
305 between CHA and the previous stack, 0.95 between CLA and the previous stack, 0.71 between XEV and
306 the previous stack and finally, 0.53 between MIC and the previous stack. These values demonstrate a
307 statistically significant correlation among the individual stalagmites and a higher correlation than between
308 the original time series. The composite δ^{18}O record was compared to the composite records from Seso (Fig.
309 A3) and Las Gloces (Fig. A4) caves and the two individual stalagmites from the other two caves (Fig. 3).
310 This comparison shows that many of the main features of the original records are also well recorded in the
311 composite (Fig. 3). One example is the interval 530-550 CE during the Dark Ages characterized by
312 relatively low δ^{18}O values in Las Gloces and Pot au Feu cave records (black arrows in Fig. 3), or the interval
313 at the end of the LIA (1675-1750 CE) with less negative δ^{18}O values in Seso, B1 and Las Gloces cave
314 records (this interval is recorded in five stalagmites: CHA, XEV, TAR, LUC and ISA, Figs. A1).

4.2. Individual isotopic and Mg/Ca profiles and composite δ^{18}O record

316 The isotopic (δ^{18}O and δ^{13}C) and Mg/Ca profiles are shown for the eight stalagmites, using their StalAge
317 models (Fig. A1) for the four caves studied (Seso, Las Gloces, B1 and Pot au Feu). In general, δ^{18}O and
318 δ^{13}C are not well correlated (r=~0.3-0.4; p-values indicating no significant correlation) with the exception
319 of TAR (r > 0.8) and CHA (r=0.5). Generally, δ^{13}C is better correlated with Mg/Ca pointing to a
320 hydrological link of these proxies, via changes in prior calcite precipitation (PCP) associated with the longer
321 residence time of the water in the soil and epikarst during dry periods (Genty et al., 2006; Moreno et al.,
322 2010). A similar interpretation was suggested for other Holocene records from northeastern Spanish caves,
323 such as speleothems from Molinos-Ejulve caves in the Iberian Range (Moreno et al., 2017) and records
324 covering the last deglaciation in the Pyrenees (Bartolomé et al., 2015a). However, δ^{13}C and Mg/Ca are
325 highly variable in absolute values and patterns among caves, and further studies are required to better
326 constrain the climate-proxy transfer functions for two parameters. Therefore, we base our paleoclimate

327 interpretations on the oxygen isotopes which are known to show a more robust response to regional climate
328 change.

329 The composite $\delta^{18}O$ record for the Central Pyrenees of the last 2500 years is shown in Fig. 3. The highest
330 $\delta^{18}O$ values of last 2500 years were reached during the RP (50 BCE-250 CE). The MCA is characterized
331 by two intervals of relatively high values (900-950 CE and 1150-1250 CE) and also the LIA shows a one
332 such interval (1675-1750 CE). In contrast, the Dark Ages are characterised by consistently low values. In
333 fact, the most negative interval of last 2500 years is reached at ~520 CE, a well-known cold episode related
334 to volcanic eruptions (see section 5.2). A long interval with low $\delta^{18}O$ values corresponds to the onset of the
335 LIA (1250-1500 CE, with two very negative excursions) as well as the end of the LIA (1750-1850 CE).
336 The most remarkable feature of the MCA and LIA is the large centennial-scale variability. In fact, the LIA
337 has a clear tripartite pattern, with two intervals of low values at the onset and end and less negative values
338 in between. In contrast, the MCA pattern, although also tripartite, it is characterized by two intervals of less
339 negative values at the onset and end, and a short period of low values in between. An interval with high
340 $\delta^{18}O$ values is observed since 1950 CE (Fig. 3).

341

5. Discussion

5.1. Interpretation of $\delta^{18}O$ data

344 Under equilibrium conditions, the $\delta^{18}O$ value of speleothem carbonate is related to just two variables: the
345 $\delta^{18}O$ value of the drip water, and the cave temperature through its control on equilibrium isotope
346 fractionation between water and calcite (Lachniet, 2009). Over the CE, air temperature in a given cave
347 likely changed very little (< 1 °C corresponding to ~0.18‰ in stalagmite $\delta^{18}O$, following Tremaine et al.,
348 2011) (PAGES Hydro2k Consortium, 2017) such that the observed $\delta^{18}O$ variations in these Pyrenean
349 speleothems of more than 1‰ are governed primarily by the $\delta^{18}O$ variability of the drip water.

350 For a constant sea-surface $\delta^{18}O_{sw}$ value, as it is expected for this time period, event-scale monitoring of the
351 isotopic composition of oxygen in the rainwater ($\delta^{18}O_r$) in different areas of the Iberian Peninsula constrains
352 some of the drivers of rainfall isotopic fractionation (Moreno et al., 2021b). Recent rainfall monitoring
353 surveys in the Central Pyrenees indicate that the values of $\delta^{18}O_r$ show an interannual dependence on
354 temperature equivalent to 0.47–0.52‰/°C, depending on the site (Giménez et al., 2021; Moreno et al.,
355 2021a). This dependence is only partially offset by the empirical value of isotope fractionation during
356 calcite precipitation (−0.18‰/°C; Tremaine et al., 2011) thus allowing to consider temperature as one
357 important factor driving $\delta^{18}O$ variability. Apparently, the rainfall amount does not strongly control the
358 isotopic values at event-scale, but analysing the $\delta^{18}O_r$ variation through time, added to the strong
359 dependence on air temperature, it is clearly observed how the most intense rainfall events together with the
360 longest lasting rain events (several days) resulted in an isotopic lightening (Giménez et al., 2021). Thus, we
361 consider that dripwater $\delta^{18}O_{dw}$ is driving the $\delta^{18}O_c$ signal in the stalagmites and, very likely, air temperature
362 and precipitation amount will be modulating its variability along last 2500 years.

363 The $\delta^{18}O$ composite record, based on the combination of MIC and XEV $\delta^{18}O$ data, provides the opportunity
364 to correlate with instrumental temperature and precipitation amount data (Fig. A4 and A5). It is worth to
365 note that the chronological control of $\delta^{18}O$ data is robust at decadal-scale, thus limiting an annual accurate
366 correlation. In spite temperature records in the region of the studied caves are, unfortunately, scarce and
367 short (e.g., the Goriz hut station covers only the last 50 years, Fig. A4b) there are two exceptions. First, the
368 homogenized MAAT dataset since 1882 from the Pic du Midi de Bigorre meteorological station (2860 m
369 a.s.l. in the French Pyrenees) (Bücher and Dessens, 1991; Dessens and Bücher, 1995), which started in
370 1882 CE, is the currently longest one from the Pyrenees (Fig. A4c). And, second, the temperature and
371 precipitation reconstruction by Pérez-Zanón et al. (2017) based on 155 stations from the Central Pyrenees
372 starting in 1910 CE (Fig. A4d). Comparing the MIC and XEV $\delta^{18}O$ data with those temperature datasets a
373 significant correlation is found with Pic du Midi de Bigorre mean annual minima temperature (σ_s =0.32; p-
374 value<0.005). Likely, the other temperature records were too short to generate a significant correlation.

Additionally, when comparing our $\delta^{18}O$ stack with the HadCRU5 reconstruction for the mean Northern Hemisphere temperatures (Morice et al., 2021) (Fig. A4e), the correlation is higher and significant (σ_s =0.49; p-value<0.005). We suspect that the length of this last series (150 years) together with a large spatial scale leads to a better correlation with the speleothem composite. However, a large part of the variance remains to be explained by other factors (i.e. precipitation changes in source, seasonality or amount). Using these relationships as a guide and considering all the isotopic change related to temperature change, the observed variation of 0.30 – 0.32 ‰ in $\delta^{18}O$ of our composite would represent a change of 1°C (Fig. A4), that appears quite plausible for the studied period.

The influence of precipitation amount variability on the isotopic composition of speleothem composite is evident from 1970 to 1980 CE, a relatively cool interval in the Pyrenees but characterized by a sustained decrease in the amount of precipitation (Pérez-Zanón et al., 2017) (Fig. A5, note reversed axis for precipitation). For this interval, the relationship between the $\delta^{18}O$ composite and temperature series is reversed, as the low precipitation leads to higher $\delta^{18}O$ values (as if they represented higher air temperatures). On the contrary, a rapid increase in precipitation at ca. 1960 without any important change in temperature, results in a negative peak on the $\delta^{18}O$ speleothem composite (Fig. A5). This shows that, in spite air temperature being an important factor influencing $\delta^{18}O$ variability in speleothems from the Pyrenees, other processes such as the amount of precipitation, its seasonality distribution or even its source(s) may be also a significant controlling factor (Priestley et al., 2023; Treble et al., 2022), especially when extreme values are reached (very dry or very wet time intervals), as was indicated by rainfall studies in the Pyrenees (Giménez et al., 2021; Moreno et al., 2021a). In any case, MIC and XEV $\delta^{18}O$ data are not significantly correlated with any of the precipitation data from Fig. A5.

Finally, it is important to note that the $\delta^{18}O$ values in the different caves varied at distinct range (Fig. 3). Thus, when producing the composite record, the $\delta^{18}O$ profiles of the eight stalagmites were normalized and detrended with the aim of combining different caves. With such a procedure, comparing relative temperature changes coming from different time periods is not possible. Thus, for example, comparing the warming magnitude of the RP with the MCA or with the IE is not feasible since data were obtained from different caves and were previously normalized and detrended. Unfortunately, none of our stalagmites cover continuously from a warm period, i.e. the MCA, to current conditions to compare values. Therefore, the ability of current data to accurately quantify changes in temperature for last 2500 years in the Central Pyrenees is limited. Normalized $\delta^{18}O$ composite record is evaluated in the context of previous local, regional and global information.

5.2 Climate reconstruction for the last 2500 years

The Pyrenees is a region threatened by global warming, where the impact on biodiversity, elements of the mountain cryosphere such as glaciers or ice caves, and water resources has been increasing in recent decades (https://www.opcc-ctp.org). The $\delta^{18}O$ composite constructed using eight speleothems represents the first climate reconstruction based on speleothems for this region covering the last 2500 years and provides an excellent opportunity to reconstruct natural variability and disentangle main driving mechanisms. We compare it first with other climate series from the Pyrenees and northern Iberia (section 5.2.1) and, then, with available speleothems from Europe and western Mediterranean to obtain a regional overview (section 5.2.2). Finally, a short discussion about the potential drivers of main observed changes is provided (section 5.2.3).

5.2.1. The last 2500 years in the context of the Iberian Peninsula

Previous climate reconstructions for the CE from the Pyrenees were mostly based on lake records (e.g., González-Sampériz et al., 2017), tree-ring data (e.g., Büntgen et al., 2017), and few data from glaciers or ice caves (Moreno et al., 2021b; Oliva et al., 2018; Sancho et al., 2018; Leunda et al., 2019). Despite large variability, these records reveal a clear distinction between relatively cold (DA, LIA) and warm (RP, MCA)

421 periods, which were generally characterized by high and low lake levels, respectively. The differences and
422 similarities among Pyrenean records merit a more detailed evaluation, organized by chronological periods.

423 A. *The Iberian - Roman period in the Pyrenees.* Considering the last 2500 years, the RP stands out as a
424 clear warm period from the speleothem composite record (Fig. 4a). In the Eastern Pyrenees, Redon Lake
425 records low winter-spring temperatures with a warming trend at the end (Pla and Catalan, 2005; Pla-Rabes
426 and Catalan, 2011), whereas the summer-autumn temperatures show a transition from cold to warm
427 (Catalan et al., 2009). Not many high-resolution Pyrenean lake records exist for this period (e.g. Corella et
428 al., 2016; Vegas-Vilarrúbia et al., 2022) and dendrochronological studies in this mountain range do not
429 cover this time period. Thus, an interesting record to compare with is the A294 ice cave in the Cotiella
430 massif (Sancho et al., 2018). This 9-m thick ice is divided into intervals of low and high snow accumulation,
431 requiring moist and cold conditions to form. The fourth (and last) stage of this ice deposit indicates a high
432 accumulation rate (Fig. 4d), thus a relatively humid and cold period, from 500 BC to 62 CE. Afterwards,
433 the record stopped reflecting the onset of a warmer and drier climate (Sancho et al., 2018) associated with
434 the RP thermal maximum (Fig 4a). Recently, not yet published observations indicate the ice deposit grew
435 during the cold/wet years associated to the DA (M. Bartolomé, personal communication). In our speleothem
436 composite, the RP is represented by Las Gloces and Pot au Feu stalagmites that show less negative values
437 (Fig. 3), which suggest rather warm, and probably dry conditions in the Central Pyrenees during the RP,
438 particularly between 0 to 200 CE (Fig. 4). This is supported by data showing retreating glaciers in the
439 Pyrenees at that time (Moreno et al., 2021b).

440 B. *The Dark Ages in the Pyrenees.* This period is characterized in our speleothem composite by cold-wet
441 climates starting ca. 300 CE, with two particular cold events at 500-650 CE and 750-850 CE and a warmer-
442 drier interval in between (650-750 CE) (Fig. 4a). Pyrenean lake records also point to cold and wet conditions
443 but with a high heterogeneity and low resolution, thus preventing a detailed characterization of this time
444 period (González-Sampériz et al., 2017). For example, Estanya Lake recorded a dominant dry climate
445 between 500 and 750 CE (Fig. 4c), changing to higher lake levels afterwards (Morellón et al., 2009), a
446 pattern that is quite coherent with the speleothem composite. Proxy data from Redon Lake suggest cold
447 winter-spring temperatures in the Eastern Pyrenees during the DA (Pla and Catalan, 2005, 2011).

448 C. *The Medieval Climate Anomaly in the Pyrenees.* The large centennial-scale temperature variability
449 recorded by the speleothem composite is particularly well expressed for the MCA and the LIA, with three
450 distinct intervals of temperature changes (yellow and blue bands in Fig. 4a), thus revealing a more complex
451 pattern as previously inferred by lower resolution records (e.g., Moreno et al., 2012; Sánchez-López et al.,
452 2016). The MCA has been interpreted as a "warm and dry" climate regime in the Southern Pyrenees
453 (Morellón et al., 2012) (Fig. 4c), characterized by low lake levels and more abundant xerophytic vegetation.
454 Our new data show, however, that a colder (maybe wetter) interval between 950 and 1050 CE separated
455 two clear warm periods before (900-950 CE) and after (1150-1250 CE; Fig. 3). This cold interval was also
456 identified in the Redon Lake record as a sudden cooling about 1000 years ago (Pla and Catalan, 2005).
457 Interestingly, this cold century was not observed by an increase in heavy precipitation in the Montcortés
458 lake record (Fig. 4b).

459 D. *The Little Ice Age in the Pyrenees.* The LIA climate variability is well-characterized in the Pyrenees
460 thanks to records from glaciers, such as moraines associated with glacier advances, but also due to historical
461 documents such as pictures or old photographs (Oliva et al., 2018). The available information indicates that
462 the LIA glaciers in the Pyrenees occupied 3366 ha in 1876, just 810 ha in 1984 and these glaciers have lost
463 23.2% of their volume considering only from 2011 to 2020 (Hughes, 2018; Vidaller et al., 2021). In many
464 Pyrenean valleys, more than one moraine belt was assigned to the LIA (García-Ruiz et al., 2014) but,
465 unfortunately, the discontinuous character of these landforms and difficulties in dating them does not allow
466 to resolve the internal pattern of the LIA in the Pyrenees. A recent compilation of records across the Iberian
467 mountains proposed several climate phases during the LIA (Oliva et al., 2018), which are well-correlated
468 with our speleothem composite (Fig. 4a): A first cooling phase lasted from the onset of the LIA (ca. 1200
469 CE) until 1480 CE, followed by relatively warmer conditions from 1480 to 1570 CE. A second phase of
470 gradual cooling occurred until 1600 CE followed by very cool conditions lasting until 1715 CE and

coinciding with the Maunder Minimum (1645 – 1715CE). In our speleothem composite, this interval is well defined as a cold period but it was not the one with minimum $\delta^{18}O$ values of the LIA (Fig. 4a). The first half of the 18th century was characterized by warm conditions, supported by many records compiled by Oliva et al. (2018). After 1760 and until the end of the LIA (ca. 1850 CE), a climate deterioration and more frequent extreme climate events were described. This last cold phase is also captured by the speleothem composite and may correspond to the Dalton Minimum (1790 – 1830 CE). It is characterised by large climate variability and lasted until about 1850 CE.

E. *The Industrial Era in the Pyrenees.* The Industrial Era (IE), defined as the last 150 years, is characterized in the Pyrenean speleothem composite by low temperatures that started to increase at about 1950 CE (Fig. 4a), in response to the Great Acceleration (Steffen et al., 2015) (yellow band in Fig.4). This increase of temperature is well recorded in other Pyrenean climate archives, such as glaciers or lake records. Thus, the last 150 years were marked by a gradual glacier retreat since 1850 CE that accelerated specially after 1980 CE, considered as a "tipping point" in glacier retreat not only on a Pyrenean scale (López-Moreno et al., 2016) but also on a global scale (Beniston et al., 2018). A decrease in heavy rainfall (Fig. 4b) and an increase in salinity (Fig. 4c) are well defined in Montcortés and Estanya lake records, respectively, during the IE, indicating a decrease in the amount of precipitation in a, likely, drier scenario. Besides these two lake records, high-altitude lakes show a significant increase in primary productivity during the last decades (Vicente de Vera García et al., 2023). These recent results demonstrate the combined impacts of climate change and increased human pressure in the Pyrenees. Coherently, last 50 years are characterized by generally enriched $\delta^{18}O$ values in our speleothem record (yellow bands in Fig. 4). However, the last two decades (our record ends in 2013, the year XEV sample was collected) are not the ones with the highest $\delta^{18}O$ values (Fig. 4a) as also observed in tree-ring data from the Spanish Central Pyrenees (Büntgen et al., 2017) (Fig. 4e). One potential explanation for the lack of exceptionally high $\delta^{18}O$ values would be a slight increase in precipitation amount. Thus, precipitation reconstruction for the Pyrenees during the last two decades indicate slightly higher values than those of previous decades (Pérez-Zanón et al., 2017, Fig. A.5). Other factors, such as changes in the precipitation source or type (eg. dominance of Atlantic frontal rainfall versus Mediterranean convective episodes) may be also behind the recorded $\delta^{18}O$ values of last decades.

5.2.2. Temperature variability in W Europe and the W Mediterranean during last 2500 years

The PAGES2k European temperature record is the most recent compilation of the last two millennia at European scale (PAGES 2k Consortium, 2013) and it is coherent with our speleothem composite for the Central Pyrenees (Fig. 6). This comparison shows a synchronicity for several of the warmest intervals of the CE, such as the first centuries CE in the RP, the 1150-1250 CE period within the MCA, and the last decades (marked as orange bars in Fig. 6). There are very few high-resolution speleothem records in Europe covering the CE (Comas-Bru et al., 2020); we selected nine speleothems records in Europe and northern Africa which cover with robust chronology and decadal resolution the last 2500 years (Fig. 5). One of these records is interpreted as NAO variability (Baker et al., 2015), three are paleo-precipitation reconstructions (Ait Brahim et al., 2019; Cisneros et al., 2021; Thatcher et al., 2022) and the other five are reflecting paleo-temperature variations (Affolter et al., 2019; Fohlmeister et al., 2012; Mangini et al., 2005; Martín-Chivelet et al., 2011; Sundqvist et al., 2010). Considering these differences in the interpretation and the fact these records are from different regions with different climates (from Sweden to Morocco), dissimilar profiles of paleoclimate variability can be expected. Still, some features are comparable and can be discussed to obtain a super-regional picture.

A. *The Roman period in Europe-W Mediterranean.* In Europe, and particularly in the Mediterranean region, the RP is well-known as a warm period (e.g., McCormick et al., 2012). The average sea-surface temperature in the western Mediterranean Sea was 2°C higher than the average temperature of the late centuries (Margaritelli et al., 2020). Our composite, with high values of normalized $\delta^{18}O$ values during the whole RP, and particularly from 0-200 CE, agrees with the scenario of warm temperatures (Fig. 5i). Speleothem data from the Balearic Islands (Cisneros et al., 2021) indicate a transition from humid to dry conditions along the Iberian-RP (Fig. 5c). The dry period at the end of the RP in the Balearic record, appears in

520 agreement with a new speleothem record from northern Italy (Hu et al., 2022), suggesting that the observed
521 drying trend was a possible contribution to the collapse of the Roman Empire in 476 CE. Record from
522 Morocco (Ait Brahim et al., 2019), contrarily, marks a humid trend at the end of the RP (Fig. 5d). Similarly,
523 an increase in humidity was observed in southern Iberia during the RP (Jiménez-Moreno et al., 2013;
524 Martín-Puertas et al., 2009) thus reflecting a large spatial heterogeneity in precipitation amount when
525 comparing records from the north and south of the Mediterranean basin.

526 B. *The Dark Ages in Europe-W Mediterranean*. After the RP, the cold Dark Ages started (450-850 CE).
527 Part of this period is known as the "Late Antique Little Ice Age" (LALIA), lasting from 536 CE to 670 CE,
528 characterized by specially cold conditions in Europe (Büntgen et al., 2016). Our speleothem composite
529 shows in general cold-wet conditions, but with centennial-scale variability during the DA (Fig. 5). Three
530 clear intervals can be defined, following the $\delta^{18}O$ pattern of our composite, as well as speleothem records
531 from the Alps (Mangini et al., 2005) and Central Europe (Affolter et al., 2019; Fohlmeister et al., 2012): an
532 initial cooling phase corresponding to the LALIA (ca. 500-650 CE), a warming phase (ca. 650-750 CE)
533 and a final cooling phase right before the onset of the warming associated with the MCA (ca 750-850 CE).
534 A $\delta^{13}C$ speleothem record from three N Iberian caves (Martín-Chivelet et al., 2011) shows a warming trend
535 in the DA period but with internal variability that, within dating uncertainties, can be related to the three
536 phases defined above (Fig. 5i). It is worth noting that the period with the most negative $\delta^{18}O$ values recorded
537 in the speleothem composite from the Pyrenees corresponds to the LALIA decades, a cooling period which
538 provoked widespread social disruption in Europe, famine, and episodes of epidemic diseases (Peregrine,
539 2020).

540 C. *The Medieval Climate Anomaly in Europe-W Mediterranean*. The MCA was one of the warmest periods
541 in continental Europe (and the W Mediterranean, Lüning et al., 2019) of the CE, usually dated to 900 CE
542 to 1300 CE and characterized by warm (Goosse et al., 2012) and relatively dry conditions (Helama et al.,
543 2009). The MCA was also characterized by a general glacier retreat, mainly associated with a decline in
544 precipitation amount in the Alps (Holzhauser et al., 2016) and the Pyrenees (Moreno et al., 2021b). This
545 scenario is supported by speleothem records from Europe and the W Mediterranean (Fig. 5), which all point
546 to generally warm (Affolter et al., 2019; Fohlmeister et al., 2012; Mangini et al., 2005; Martín-Chivelet et
547 al., 2011; Sundqvist et al., 2010) and/or dry conditions (Ait Brahim et al., 2019; Baker et al., 2015; Thatcher
548 et al., 2022), even leading to speleothem growth stops as for example seen in the Balearic record (Cisneros
549 et al., 2021). Previous studies have emphasized the complexity of the spatial and seasonal structure of the
550 MCA in Europe (Goosse et al., 2012). The selected speleothem records underscore this complexity,
551 particularly considering that in our Pyrenean composite one of the periods marked as cold-wet occurred
552 during the MCA, ca. 950-1050 CE (Fig. 5). We propose that this cold interval represents the climate
553 response to the Oort solar minimum in the Pyrenees, a time period characterized by low number of sunspots
554 covering spanning 1010 to 1050 CE (Bard et al., 2000).

555 D. *The Little Ice Age in Europe-W Mediterranean*. The LIA is well known in Europe and the W
556 Mediterranean region, characterized by cold temperatures and relatively humid conditions as recorded, for
557 example, in chironomid-inferred summer temperatures (Ilyashuk et al., 2019), Mediterranean SSTs
558 (Cisneros et al., 2016), the advance of alpine glaciers (Holzhauser et al., 2016) and the rise of lake levels
559 (Magny, 2013). The LIA cooling, however, was not continuous and uniform in space and time. Regarding
560 temperatures, many of the available reconstructions from the Alps (Trachsel et al., 2012), Scandinavia
561 (Zawiska et al., 2017), and other regions of Europe (Luterbacher et al., 2016), provide evidence for a main
562 LIA cooling phase which was divided into three parts: two cold intervals with a slightly warmer episode in
563 between, with the most severe cooling during the 18th century (Ilyashuk et al., 2019). This pattern is also
564 found in the two temperature records from Iberian speleothems (this study and the one from Martín-
565 Chivelet et al., 2011) and a temperature record from the Alps (Mangini et al., 2005) (Fig. 5, marked by
566 arrows). The other European speleothem records show only two phases during the LIA: a longer and intense
567 cooling period followed by a warming (Fig. 5, Affolter et al., 2019; Fohlmeister et al., 2012; Sundqvist et
568 al., 2010). A tripartite pattern is recorded by humidity-sensitive speleothems from Portugal, with wet-dry-
569 wet conditions in excellent agreement with the cold-warm-cold pattern in the Pyrenean record (this study),

supporting the concept that this pattern is controlled by changes in intensity and N-S migration of the Azores High (Thatcher et al., 2022).

E. *The Industrial Era in Europe-W Mediterranean.* Between about 1870 CE and today, an increase in temperature is detected by European speleothem records (Fig. 5), as previously shown by the retreat of European glaciers (Beniston et al., 2018) and tree-ring summer temperature records (Büntgen et al., 2011) as well as drought reconstructions (Büntgen et al., 2021). The impacts in Europe and the W Mediterranean of the current global warming trend, accelerated during last 50 years, are becoming more and more evident (Jacob et al., 2018; Naumann et al., 2021).

5.2.3 Drivers of past temperature variability in the Pyrenees

The good correlation and synchronicity between the PAGES2k European record and the Pyrenean composite (marked as orange bars in Fig. 6) supports the interpretation of temperature being the dominant factor in controlling the speleothem record. This centennial-scale correlation can be extended to a worldwide tree-ring compilation (Sigl et al., 2015) pointing to the presence of common warm periods in the Central Pyrenees. Interestingly, if precipitation amount was the dominant factor controlling the $\delta^{18}O$ speleothem composite, it would be difficult to find a common signal at regional or even continental scale, as indicated by the overall good correlation shown in Fig. 6.

It is worth to mention the good correlation with several especially cold periods at decadal scale (blue bars in Fig. 6), such as the event at 540-550 CE (registered at 520 CE in the speleothem record) or two cold spikes at 800-850 CE at the end of the DA. We proposed that the cold event at ca. 540 CE (the coldest of the speleothem record) is related to a cataclysmic volcanic eruption that took place in Iceland in 536 CE and spewed ash across the Northern Hemisphere, together with the effect of two other massive eruptions in 540 and 547 CE (Fig. 6b, Sigl et al., 2015). An unprecedented, long-lasting and spatially synchronized cooling was observed in European tree-ring records associated with these large volcanic eruptions, corresponding to the LALIA period (Büntgen et al., 2016). Therefore, volcanic events, at least the large ones such that from 536 CE in Iceland, have an effect driving temperature variations in the Pyrenean region.

There is also an evident synchrony between the European record and the Pyrenean speleothems in several of the more recent coldest intervals of the MCA and the LIA (dark blue bars in Fig. 6), probably a regional response to minima in solar irradiance as these events correspond to minima in sunspot numbers (Fig. 6c, (Usoskin et al., 2014, 2016): 1010-1050 CE (Oort minimum), 1280-1350 CE (Wolf minimum), 1450-1550 CE (Spörer minimum), 1645-1715 CE (Maunder minimum) and 1790-1820 CE (Dalton minimum). Because variations in total solar irradiance are relatively small, on the order of a few tenths of Wm^{-2}, the mechanism that could result in a detectable cooling remains uncertain (Gray et al., 2010). While some studies discarded the idea that there has been a strong direct radiative influence of solar forcing on Northern Hemisphere temperatures in the past millennium (Schurer et al., 2014), other authors demonstrated a connection among solar variability and climate throughout changes in the large-scale atmospheric circulation of the Northern Hemisphere, such as the North Atlantic Oscillation (NAO) (Martin-Puertas et al., 2012). The NAO was proposed as a plausible mechanism to explain climate changes in Europe during the MCA vs LIA periods through the study in combination of proxy records and model simulations (Trouet et al., 2009; Mann et al., 2009). Thus, it was postulated that the MCA/LIA transition included a weakening of the Atlantic Meridional Overturning Circulation (AMOC) and a transition to more negative NAO conditions, resulting in a strong cooling of the North Atlantic region and an increase in the storm intensity (Trouet et al., 2012).

Such a connection among solar irradiance and temperature over Europe is then manifested through a change in the pressure gradient in the Atlantic that resembles a negative phase of the NAO and results in lower temperatures over Europe but also in a southward shift of the storm tracks enhancing precipitation amount over central and southern Europe (Swingedouw et al., 2011). As solar irradiance decreases, colder temperatures over the Northern Hemisphere continents are observed, especially in winter (1° to 2°C), in agreement with historical records and proxy data for surface temperatures (Shindell et al., 2001).

618 Coherently, most episodes of flooding in northwest and northern Europe region match with multi-decadal
619 periods of grand solar minima and are thus also associated to the negative phase in the NAO index (Benito
620 et al., 2015) (Fig. 6d).

621 In Iberia, the NAO index was embraced to explain the dryness during the MCA as observed in low
622 resolution records (Moreno et al., 2012). Further studies based on proxy reconstructions in Iberia explained
623 those MCA - LIA differences by using interactions between the NAO and the East Atlantic (EA) phases
624 (Sánchez-López et al., 2016). In that line, the persistence of NAO phases, for example, the dominance of
625 positive index during Medieval times, has been questioned (Ortega et al., 2015) and the interactions with
626 other atmospheric modes, together with the non-stationary character of these atmospheric patterns, are
627 nowadays important issues to contemplate when providing a NAO reconstruction (Comas-Bru and
628 Hernández, 2018). In Fig. 6g, the NAO reconstruction provided using a lake record in NW Iberia
629 (Hernández et al., 2020) is compared with the speleothem Pyrenean record demonstrating a good
630 connection. Not surprisingly, the lack of correlation for some periods could be associated to i) chronological
631 uncertainties of both records, ii) different season recorded by the analyzed proxies and iii) distinct influence
632 of NAO in W and E of the IP.

6. Conclusions

634 The eight stalagmites presented in this study document for the first-time significant climate changes on the
635 decadal scale in the Central Pyrenees during the last 2500 years. The $\delta^{18}O$ composite record is dominated
636 by regional temperature changes, as suggested by monitoring data and by the correlation with observational
637 temperature data from the Pyrenees and at a hemispheric scale. The precipitation amount may also play a
638 role as shown by the comparison with Pyrenean lake records.

639 On a regional scale, there is a good agreement with other Pyrenean and Iberian records (lake levels, tree
640 rings and glacier advances) indicating a regional representativity of this new record. The RP stands out as
641 a clear warm period, while the DA, MCA and LIA exhibit a high centennial-scale variability with cold
642 (e.g., 520-540 CE and 1750-1850 CE) and warm intervals (e.g., 900-950 CE and 1150-1250 CE) modulated
643 by increases and decreases in the precipitation amount, respectively. In spite temperature increases since
644 1950 CE, known as the Great Acceleration within the IE, the last two decades are not the ones with the
645 highest $\delta^{18}O$ values in the composite record, likely pointing to the secondary role played by precipitation
646 amount.

647 On a European scale, the Pyrenean composite is in robust agreement with the PAGES2k temperature
648 reconstructions, particularly during warm events. It shows some similarities with other speleothem
649 reconstructions from the Alps, Central and Northern Europe pointing to coherent patterns all over the
650 continent for cold/wet and warm/dry periods of last 2500 years. This coherence is supported by synchronous
651 changes with the sunspot number (low temperatures during solar minima), the North Atlantic Oscillation
652 index (low NAO correlates with cold and wet decades) and major volcanic eruptions (e.g., several eruptions
653 during LALIA).

654 **Author contribution.** MB, AM and CS designed the study; MB, AB and CS carried out the field work;
655 MB, JH, IC, HS and NH did the analyses. LE and HC provided the U-Th facilities. MB and AM prepared
656 the manuscript with contributions from all co-authors.

657 **Competing interests:** The authors declare that they have no conflict of interest.

658 **Acknowledgements.** We acknowledge the Spanish projects CTM2013-48639-C2-2-R (OPERA),
659 CGL2016-77479-R (SPYRIT), and PID2019–106050RB-I00 (PYCACHU) for funding. We thank the
660 Ordesa y Monte Perdido National Park (Spain) authorities and guards for their permission and help in
661 exploring and monitoring the studied caves. We also thank Jaime Mas and Xavier Fuertes (Free Caving
662 Team and GEB), Ramón Queraltó and Carles Pons (Asociación Científica Espeleológica Cotiella), Maria
663 Leunda and the Palazio family (www.hotelpalazio.com) for their invaluable help during fieldwork. Dr.

664   Miguel Sevilla (IPE-CSIC) is greatly acknowledge for his design and production of maps in Fig. 1. The
665   authors would like to acknowledge the use of the Servicio General de Apoyo a la Investigación-SAI,
666   University of Zaragoza. This study contributes to the work carried out by the DGA research group Procesos
667   Geoambientales y Cambio Global (ref.: E02-20R). Miguel Bartolomé is supported by the HORIZON TMA
668   MSCA Postdoctoral Fellowships - Global Fellowships 2022 MODKARST project (nº 101107943) funded
669   by the European Union. Isabel Cacho thanks the Catalan Institution for Research and Advanced Studies
670   (ICREA) academia program from the Generalitat de Catalunya.

671   **References**

672   Abrantes, F., Rodrigues, T., Rufino, M., Salgueiro, E., Oliveira, D., Gomes, S., Oliveira, P., Costa,
673   A., Mil-Homens, M., Drago, T., and Naughton, F.: The climate of the Common Era off the
674   Iberian Peninsula, Clim. Past, 13, 1901–1918, https://doi.org/10.5194/cp-13-1901-2017, 2017.

675   Affolter, S., Häuselmann, A., Fleitmann, D., Edwards, R. L., Cheng, H., and Leuenberger, M.:
676   Central Europe temperature constrained by speleothem fluid inclusion water isotopes over the
677   past 14,000 years, Science Advances, 5, eaav3809, https://doi.org/10.1126/sciadv.aav3809,
678   2019.

679   Ahmed, M., Anchukaitis, K. J., Asrat, A., Borgaonkar, H. P., Braida, M., Buckley, B. M., Büntgen,
680   U., Chase, B. M., Christie, D. A., Cook, E. R., Curran, M. A. J., Diaz, H. F., Esper, J., Fan, Z.-X.,
681   Gaire, N. P., Ge, Q., Gergis, J., González-Rouco, J. F., Goosse, H., Grab, S. W., Graham, N.,
682   Graham, R., Grosjean, M., Hanhijärvi, S. T., Kaufman, D. S., Kiefer, T., Kimura, K., Korhola, A. A.,
683   Krusic, P. J., Lara, A., Lézine, A.-M., Ljungqvist, F. C., Lorrey, A. M., Luterbacher, J., Masson-
684   Delmotte, V., McCarroll, D., McConnell, J. R., McKay, N. P., Morales, M. S., Moy, A. D.,
685   Mulvaney, R., Mundo, I. A., Nakatsuka, T., Nash, D. J., Neukom, R., Nicholson, S. E., Oerter, H.,
686   Palmer, J. G., Phipps, S. J., Prieto, M. R., Rivera, A., Sano, M., Severi, M., Shanahan, T. M., Shao,
687   X., Shi, F., Sigl, M., Smerdon, J. E., Solomina, O. N., Steig, E. J., Stenni, B., Thamban, M., Trouet,
688   V., Turney, C. S. M., Umer, M., van Ommen, T., Verschuren, D., Viau, A. E., Villalba, R., Vinther,
689   B. M., von Gunten, L., Wagner, S., Wahl, E. R., Wanner, H., Werner, J. P., White, J. W. C., Yasue,
690   K., Zorita, E., and PAGES 2k Consortium: Continental-scale temperature variability during the
691   past two millennia, Nature Geoscience, 6, 339–346, https://doi.org/10.1038/ngeo1797, 2013.

692   Ait Brahim, Y., Wassenburg, J. A., Sha, L., Cruz, F. W., Deininger, M., Sifeddine, A., Bouchaou, L.,
693   Spötl, C., Edwards, R. L., and Cheng, H.: North Atlantic Ice-Rafting, Ocean and Atmospheric
694   Circulation During the Holocene: Insights From Western Mediterranean Speleothems,
695   Geophysical Research Letters, 46, 7614–7623, https://doi.org/10.1029/2019GL082405, 2019.

696   Baker, A., C. Hellstrom, J., Kelly, B. F. J., Mariethoz, G., and Trouet, V.: A composite annual-
697   resolution stalagmite record of North Atlantic climate over the last three millennia, Sci Rep, 5,
698   10307, https://doi.org/10.1038/srep10307, 2015.

699   Bard, E., Raisbeck, G., Yiou, F., and Jouzel, J.: Solar irradiance during the last 1200 years based
700   on cosmogenic nuclides, Tellus B, 52, 985–992, https://doi.org/10.1034/j.1600-0889.2000.d01-
701   7.x, 2000.

702   Bartolomé, M.: La Cueva del Caserío de Seso (Pirineo Central): espeleogénesis, dinámica actual
703   y reconstrucción paleoambiental de los últimos 13.000 años, Universidad de Zaragoza, 276 pp.,
704   2016.

705   Bartolomé, M., Moreno, A., Sancho, C., Stoll, H. M., Cacho, I., Spötl, C., Belmonte, Á., Edwards,
706   R. L., Cheng, H., and Hellstrom, J. C.: Hydrological change in Southern Europe responding to

707 increasing North Atlantic overturning during Greenland Stadial 1, PNAS, 112, 6568–6572,
708 https://doi.org/10.1073/pnas.1503990112, 2015a.

709 Bartolomé, M., Sancho, C., Moreno, A., Oliva-Urcia, B., Belmonte, Á., Bastida, J., Cheng, H., and
710 Edwards, R. L.: Upper Pleistocene interstratal piping-cave speleogenesis: The Seso Cave System
711 (Central Pyrenees, Northern Spain), Geomorphology, 228, 335–344,
712 https://doi.org/10.1016/j.geomorph.2014.09.007, 2015b.

713 Beniston, M., Farinotti, D., Stoffel, M., Andreassen, L. M., Coppola, E., Eckert, N., Fantini, A.,
714 Giacona, F., Hauck, C., Huss, M., Huwald, H., Lehning, M., López-Moreno, J.-I., Magnusson, J.,
715 Marty, C., Morán-Tejéda, E., Morin, S., Naaim, M., Provenzale, A., Rabatel, A., Six, D., Stötter,
716 J., Strasser, U., Terzago, S., and Vincent, C.: The European mountain cryosphere: a review of its
717 current state, trends, and future challenges, The Cryosphere, 12, 759–794,
718 https://doi.org/10.5194/tc-12-759-2018, 2018.

719 Benito, G., Macklin, M. G., Panin, A., Rossato, S., Fontana, A., Jones, A. F., Machado, M. J.,
720 Matlakhova, E., Mozzi, P., and Zielhofer, C.: Recurring flood distribution patterns related to
721 short-term Holocene climatic variability, Sci Rep, 5, 16398, https://doi.org/10.1038/srep16398,
722 2015.

723 Bernal-Wormull, J. L., Moreno, A., Pérez-Mejías, C., Bartolomé, M., Aranburu, A.,
724 Arriolabengoa, M., Iriarte, E., Cacho, I., Spötl, C., Edwards, R. L., and Cheng, H.: Immediate
725 temperature response in northern Iberia to last deglacial changes in the North Atlantic,
726 Geology, https://doi.org/10.1130/G48660.1, 2021.

727 Bücher, A. and Dessens, J.: Secular Trend of Surface Temperature at an Elevated Observatory
728 in the Pyrenees, Journal of Climate, 4, 859–868, https://doi.org/10.1175/1520-
729 0442(1991)004<0859:STOSTA>2.0.CO;2, 1991.

730 Büntgen, U., Tegel, W., Nicolussi, K., McCormick, M., Frank, D., Trouet, V., Kaplan, J. O., Herzig,
731 F., Heussner, K.-U., Wanner, H., Luterbacher, J., and Esper, J.: 2500 Years of European Climate
732 Variability and Human Susceptibility, Science, 2011.

733 Büntgen, U., Myglan, V. S., Ljungqvist, F. C., McCormick, M., Di Cosmo, N., Sigl, M., Jungclaus,
734 J., Wagner, S., Krusic, P. J., Esper, J., Kaplan, J. O., de Vaan, M. A. C., Luterbacher, J., Wacker, L.,
735 Tegel, W., and Kirdyanov, A. V.: Cooling and societal change during the Late Antique Little Ice
736 Age from 536 to around 660 AD, Nature Geosci, 9, 231–236,
737 https://doi.org/10.1038/ngeo2652, 2016.

738 Büntgen, U., Krusic, P. J., Verstege, A., Sangüesa-Barreda, G., Wagner, S., Camarero, J. J.,
739 Ljungqvist, F. C., Zorita, E., Oppenheimer, C., Konter, O., Tegel, W., Gärtner, H., Cherubini, P.,
740 Reinig, F., and Esper, J.: New Tree-Ring Evidence from the Pyrenees Reveals Western
741 Mediterranean Climate Variability since Medieval Times, J. Climate, 30, 5295–5318,
742 https://doi.org/10.1175/JCLI-D-16-0526.1, 2017.

743 Büntgen, U., Urban, O., Krusic, P. J., Rybníček, M., Kolář, T., Kyncl, T., Ač, A., Koňasová, E.,
744 Čáslavský, J., Esper, J., Wagner, S., Saurer, M., Tegel, W., Dobrovolný, P., Cherubini, P., Reinig,
745 F., and Trnka, M.: Recent European drought extremes beyond Common Era background
746 variability, Nat. Geosci., 14, 190–196, https://doi.org/10.1038/s41561-021-00698-0, 2021.

747 Cisneros, M., Cacho, I., Frigola, J., Canals, M., Masqué, P., Martrat, B., Casado, M., Grimalt, J.
748 O., Pena, L. D., Margaritelli, G., and Lirer, F.: Sea surface temperature variability in the central-

749 western Mediterranean Sea during the last 2700 years: a multi-proxy and multi-record
750 approach, Clim. Past, 12, 849–869, https://doi.org/10.5194/cp-12-849-2016, 2016.

751 Cisneros, M., Cacho, I., Moreno, A., Stoll, H., Torner, J., Català, A., Edwards, R. L., Cheng, H.,
752 and Fornós, J. J.: Hydroclimate variability during the last 2700 years based on stalagmite multi-
753 proxy records in the central-western Mediterranean, Quaternary Science Reviews, 269,
754 107137, https://doi.org/10.1016/j.quascirev.2021.107137, 2021.

755 Comas-Bru, L. and Hernández, A.: Reconciling North Atlantic climate modes: revised monthly
756 indices for the East Atlantic and the Scandinavian patterns beyond the 20th century, Earth
757 System Science Data, 10, 2329–2344, https://doi.org/10.5194/essd-10-2329-2018, 2018.

758 Comas-Bru, L., Rehfeld, K., Roesch, C., Amirnezhad-Mozhdehi, S., Harrison, S. P.,
759 Atsawawaranunt, K., Ahmad, S. M., Brahim, Y. A., Baker, A., Bosomworth, M., Breitenbach, S.
760 F. M., Burstyn, Y., Columbu, A., Deininger, M., Demény, A., Dixon, B., Fohlmeister, J., Hatvani, I.
761 G., Hu, J., Kaushal, N., Kern, Z., Labuhn, I., Lechleitner, F. A., Lorrey, A., Martrat, B., Novello, V.
762 F., Oster, J., Pérez-Mejías, C., Scholz, D., Scroxton, N., Sinha, N., Ward, B. M., Warken, S.,
763 Zhang, H., and SISAL Working Group members: SISALv2: a comprehensive speleothem isotope
764 database with multiple age–depth models, Earth System Science Data, 12, 2579–2606,
765 https://doi.org/10.5194/essd-12-2579-2020, 2020.

766 Corella, J. P., Valero-Garcés, B. L., Vicente- Serrano, S. M., Brauer, A., and Benito, G.: Three
767 millennia of heavy rainfalls in Western Mediterranean: frequency, seasonality and atmospheric
768 drivers, Scientific Reports, 6, https://doi.org/10.1038/srep38206, 2016.

769 Dessens, J. and Bücher, A.: Changes in minimum and maximum temperatures at the Pic du
770 Midi in relation with humidity and cloudiness, 1882–1984, Atmospheric Research, 37, 147–
771 162, https://doi.org/10.1016/0169-8095(94)00075-O, 1995.

772 Edwards, R. L., Chen, J. H., and Wasserburg, G. J.: 238U-234U-230Th-232Th systematics and
773 the precise measurements of time over the past 500.000 years, Earth and Planetary Science
774 Letters, 81, 175–192, 1987.

775 Fohlmeister, J.: A statistical approach to construct composite climate records of dated
776 archives, Quaternary Geochronology, 14, 48–56,
777 https://doi.org/10.1016/j.quageo.2012.06.007, 2012.

778 Fohlmeister, J., Kromer, B., and Mangini, A.: The influence of soil organic matter age spectrum
779 on the reconstruction of atmospheric 14C levels via stalagmites, Radiocarbon, 53, 99–115,
780 https://doi.org/10.1017/S003382220003438X, 2011.

781 Fohlmeister, J., Schröder-Ritzrau, A., Scholz, D., Spötl, C., Riechelmann, D. F. C., Mudelsee, M.,
782 Wackerbarth, A., Gerdes, A., Riechelmann, S., Immenhauser, A., Richter, D. K., and Mangini, A.:
783 Bunker Cave stalagmites: an archive for central European Holocene climate variability, Clim.
784 Past, 8, 1751–1764, https://doi.org/10.5194/cp-8-1751-2012, 2012.

785 García-Ruiz, J. M., Palacios, D., Andrés, N. de, Valero-Garcés, B. L., López-Moreno, J. I., and
786 Sanjuán, Y.: Holocene and 'Little Ice Age' glacial activity in the Marboré Cirque, Monte Perdido
787 Massif, Central Spanish Pyrenees, The Holocene, 24, 1439–1452,
788 https://doi.org/10.1177/0959683614544053, 2014.

789 Genty, D., Vokal, B., Obelic, B., and Massault, M.: Bomb 14C time history recorded in two
790 modern stalagmites — importance for soil organic matter dynamics and bomb 14C distribution

791   over continents, Earth and Planetary Science Letters, 160, 795–809,
792   https://doi.org/10.1016/S0012-821X(98)00128-9, 1998.

793   Genty, D., Blamart, D., Ghaleb, B., Plagnes, V., Causse, Ch., Bakalowicz, M., Zouari, K., Chkir, N.,
794   Hellstrom, J., Wainer, K., and Bourges, F.: Timing and dynamics of the last deglaciation from
795   European and North African δ13C stalagmite profiles—comparison with Chinese and South
796   Hemisphere stalagmites, Quaternary Science Reviews, 25, 2118–2142,
797   https://doi.org/10.1016/j.quascirev.2006.01.030, 2006.

798   Genty, D., Labuhn, I., Hoffmann, G., Danis, P. A., Mestre, O., Bourges, F., Wainer, K., Massault,
799   M., Van Exter, S., Régnier, E., Orengo, Ph., Falourd, S., and Minster, B.: Rainfall and cave water
800   isotopic relationships in two South-France sites, Geochimica et Cosmochimica Acta, 131, 323–
801   343, https://doi.org/10.1016/j.gca.2014.01.043, 2014.

802   Giménez, R., Bartolomé, M., Gázquez, F., Iglesias, M., and Moreno, A.: Underlying Climate
803   Controls in Triple Oxygen (16 O, 17 O, 18 O) and Hydrogen (1 H, 2 H) Isotopes Composition of
804   Rainfall (Central Pyrenees), Front. Earth Sci., 9, https://doi.org/10.3389/feart.2021.633698,
805   2021.

806   González-Sampériz, P., Aranbarri, J., Pérez-Sanz, A., Gil-Romera, G., Moreno, A., Leunda, M.,
807   Sevilla-Callejo, M., Corella, J. P., Morellón, M., Oliva, B., and Valero-Garcés, B.: Environmental
808   and climate change in the southern Central Pyrenees since the Last Glacial Maximum: A view
809   from the lake records, CATENA, 149, 668–688, 2017.

810   Goosse, H., Guiot, J., Mann, M. E., Dubinkina, S., and Sallaz-Damaz, Y.: The medieval climate
811   anomaly in Europe: Comparison of the summer and annual mean signals in two
812   reconstructions and in simulations with data assimilation, Global and Planetary Change, 84–85,
813   35–47, https://doi.org/10.1016/j.gloplacha.2011.07.002, 2012.

814   Gray, L. J., Beer, J., Geller, M., Haigh, J. D., Lockwood, M., Matthes, K., Cubasch, U., Fleitmann,
815   D., Harrison, G., Hood, L., Luterbacher, J., Meehl, G. A., Shindell, D., van Geel, B., and White,
816   W.: Solar influences on climate, Rev. Geophys., 48, RG4001, 2010.

817   Hammer, O., Harper, D. A. T., and Ryan, P. D.: PAST: Paleontological statistics software package
818   for education and data analysis. 4(1): 9pp., Palaeontologia Electronica, 4 (1), 9, 2001.

819   Helama, S., Meriläinen, J., and Tuomenvirta, H.: Multicentennial megadrought in northern
820   Europe coincided with a global El Niño–Southern Oscillation drought pattern during the
821   Medieval Climate Anomaly, Geology, 37, 175–178, https://doi.org/10.1130/G25329A.1, 2009.

822   Hellstrom, J.: U–Th dating of speleothems with high initial 230Th using stratigraphical
823   constraint, Quaternary Geochronology, 1, 289–295,
824   https://doi.org/10.1016/j.quageo.2007.01.004, 2006.

825   Hernández, A., Sánchez-López, G., Pla-Rabes, S., Comas-Bru, L., Parnell, A., Cahill, N., Geyer, A.,
826   Trigo, R. M., and Giralt, S.: A 2,000-year Bayesian NAO reconstruction from the Iberian
827   Peninsula, Sci Rep, 10, 14961, https://doi.org/10.1038/s41598-020-71372-5, 2020.

828   Holzhauser, H., Magny, M., and Zumbuühl, H. J.: Glacier and lake-level variations in west-
829   central Europe over the last 3500 years:, The Holocene,
830   https://doi.org/10.1191/0959683605hl853ra, 2016.

831   Hu, H.-M., Michel, V., Valensi, P., Mii, H.-S., Starnini, E., Zunino, M., and Shen, C.-C.: Stalagmite-
832   Inferred Climate in the Western Mediterranean during the Roman Warm Period, Climate, 10,
833   93, https://doi.org/10.3390/cli10070093, 2022.

834   Hua, Q., McDonald, J., Redwood, D., Drysdale, R., Lee, S., Fallon, S., and Hellstrom, J.: Robust
835   chronological reconstruction for young speleothems using radiocarbon, Quaternary
836   Geochronology, 14, 67–80, https://doi.org/10.1016/j.quageo.2012.04.017, 2012.

837   Hua, Q., Cook, D., Fohlmeister, J., Penny, D., Bishop, P., and Buckman, S.: Radiocarbon Dating
838   of a Speleothem Record of Paleoclimate for Angkor, Cambodia, Radiocarbon, 59, 1873–1890,
839   https://doi.org/10.1017/RDC.2017.115, 2017.

840   Hughes, P. D.: Little Ice Age glaciers and climate in the Mediterranean mountains: a new
841   analysis, CIG, 44, 15, https://doi.org/10.18172/cig.3362, 2018.

842   Ilyashuk, E. A., Heiri, O., Ilyashuk, B. P., Koinig, K. A., and Psenner, R.: The Little Ice Age
843   signature in a 700-year high-resolution chironomid record of summer temperatures in the
844   Central Eastern Alps, Clim Dyn, 52, 6953–6967, https://doi.org/10.1007/s00382-018-4555-y,
845   2019.

846   IPCC, 2021: Climate Change 2021: The Physical Science Basis. Contribution of Working Group I
847   to the Sixth Assessment Report of the Intergovernmental Panel on Climate Change [Masson-
848   Delmotte, V., P. Zhai, A. Pirani, S.L. Connors, C. Péan, S. Berger, N. Caud, Y. Chen, L. Goldfarb,
849   M.I. Gomis, M. Huang, K. Leitzell, E. Lonnoy, J.B.R. Matthews, T.K. Maycock, T. Waterfield, O.
850   Yelekçi, R. Yu, and B. Zhou (eds.)]. Cambridge University Press, Cambridge, United Kingdom
851   and New York, NY, USA, 2391 pp.doi:10.1017/9781009157896.

852   Jacob, D., Kotova, L., Teichmann, C., Sobolowski, S. P., Vautard, R., Donnelly, C., Koutroulis, A.
853   G., Grillakis, M. G., Tsanis, I. K., Damm, A., Sakalli, A., and van Vliet, M. T. H.: Climate Impacts in
854   Europe Under +1.5°C Global Warming, Earth's Future, 6, 264–285,
855   https://doi.org/10.1002/2017EF000710, 2018.

856   Jiménez-Moreno, G., García-Alix, A., Hernández-Corbalán, M. D., Anderson, R. S., and Delgado-
857   Huertas, A.: Vegetation, fire, climate and human disturbance history in the southwestern
858   Mediterranean area during the late Holocene, Quaternary Research, 79, 110–122,
859   https://doi.org/10.1016/j.yqres.2012.11.008, 2013.

860   Konecky, B. L., McKay, N. P., Churakova (Sidorova), O. V., Comas-Bru, L., Dassié, E. P., DeLong,
861   K. L., Falster, G. M., Fischer, M. J., Jones, M. D., Jonkers, L., Kaufman, D. S., Leduc, G.,
862   Managave, S. R., Martrat, B., Opel, T., Orsi, A. J., Partin, J. W., Sayani, H. R., Thomas, E. K.,
863   Thompson, D. M., Tyler, J. J., Abram, N. J., Atwood, A. R., Conroy, J. L., Kern, Z., Porter, T. J.,
864   Stevenson, S. L., von Gunten, L., and the Iso2k Project Members: The Iso2k Database: A global
865   compilation of paleo-δ^{18}O and δ^2H records to aid understanding of Common Era climate, Earth
866   System Science Data Discussions, 1–49, https://doi.org/10.5194/essd-2020-5, 2020.

867   Lachniet, M. S.: Climatic and environmental controls on speleothem oxygen-isotope values,
868   Quaternary Science Reviews, 28, 412–432, 2009.

869   Leunda, M., González-Sampériz, P., Gil-Romera, G., Bartolomé, M., Belmonte-Ribas, Á., Gómez-
870   García, D., Kaltenrieder, P., Rubiales, J. M., Schwörer, C., Tinner, W., Morales-Molino, C., and
871   Sancho, C.: Ice cave reveals environmental forcing of long-term Pyrenean tree line dynamics,
872   Journal of Ecology, 107, 814–828, https://doi.org/10.1111/1365-2745.13077, 2019.

873 López-Moreno, J. I., Revuelto, J., Rico, I., Chueca-Cía, J., Julián, A., Serreta, A., Serrano, E.,
874 Vicente-Serrano, S. M., Azorin-Molina, C., Alonso-González, E., and García-Ruiz, J. M.: Thinning
875 of the Monte Perdido Glacier in the Spanish Pyrenees since 1981, The Cryosphere, 10, 681–
876 694, https://doi.org/10.5194/tc-10-681-2016, 2016.

877 López-Moreno, J. I., García-Ruiz, J. M., Vicente-Serrano, S. M., Alonso-González, E., Revuelto-
878 Benedí, J., Rico, I., Izagirre, E., and Beguería-Portugués, S.: Critical discussion of: "A farewell to
879 glaciers: Ecosystem services loss in the Spanish Pyrenees," Journal of Environmental
880 Management, 275, 111247, https://doi.org/10.1016/j.jenvman.2020.111247, 2020.

881 Lüning, S., Schulte, L., Garcés-Pastor, S., Danladi, I. b., and Gałka, M.: The Medieval Climate
882 Anomaly in the Mediterranean Region, Paleoceanography and Paleoclimatology, 34, 1625–
883 1649, https://doi.org/10.1029/2019PA003734, 2019.

884 Luterbacher, J., Werner, J. P., Smerdon, J. E., Fernández-Donado, L., González-Rouco, F. J.,
885 Barriopedro, D., Ljungqvist, F. C., Büntgen, U., Zorita, E., Wagner, S., Esper, J., McCarroll, D.,
886 Toreti, A., Frank, D., Jungclaus, J. H., M Barriendos, Bertolin, C., Bothe, O., Brázdil, R., Camuffo,
887 D., Dobrovolný, P., Gagen, M., García-Bustamante, E., Ge, Q., Gómez-Navarro, J. J., Guiot, J.,
888 Hao, Z., Hegerl, G. C., Holmgren, K., Klimenko, V. V., Martín-Chivelet, J., Pfister, C., N Roberts,
889 Schindler, A., Schurer, A., Solomina, O., Gunten, L. von, Wahl, E., Wanner, H., Wetter, O.,
890 Xoplaki, E., Yuan, N., D Zanchettin, Zhang, H., and Zerefos, C.: European summer temperatures
891 since Roman times, Environ. Res. Lett., 11, 024001, https://doi.org/10.1088/1748-
892 9326/11/2/024001, 2016.

893 Magny, M.: Orbital, ice-sheet, and possible solar forcing of Holocene lake-level fluctuations in
894 west-central Europe: A comment on Bleicher, The Holocene,
895 https://doi.org/10.1177/0959683613483627, 2013.

896 Mangini, A., Spötl, C., and Verdes, P.: Reconstruction of temperature in the Central Alps during
897 the past 2000 yr from a δ18O stalagmite record, Earth and Planetary Science Letters, 235, 741–
898 751, https://doi.org/10.1016/j.epsl.2005.05.010, 2005.

899 Mann, M. E.: Beyond the hockey stick: Climate lessons from the Common Era, PNAS, 118,
900 https://doi.org/10.1073/pnas.2112797118, 2021.

901 Mann, M. E., Zhang, Z., Rutherford, S., Bradley, R. S., Hughes, M. K., Shindell, D., Ammann, C.,
902 Faluvegi, G., and Ni, F.: Global Signatures and Dynamical Origins of the Little Ice Age and
903 Medieval Climate Anomaly, Science, 326, 1256–1260, 2009.

904 Margaritelli, G., Cacho, I., Català, A., Barra, M., Bellucci, L. G., Lubritto, C., Rettori, R., and Lirer,
905 F.: Persistent warm Mediterranean surface waters during the Roman period, Sci Rep, 10,
906 10431, https://doi.org/10.1038/s41598-020-67281-2, 2020.

907 Markowska, M., Fohlmeister, J., Treble, P. C., Baker, A., Andersen, M. S., and Hua, Q.:
908 Modelling the 14C bomb-pulse in young speleothems using a soil carbon continuum model,
909 Geochimica et Cosmochimica Acta, 261, 342–367, https://doi.org/10.1016/j.gca.2019.04.029,
910 2019.

911 Martín-Chivelet, J., Muñoz-García, M. B., Edwards, R. L., Turrero, M. J., and Ortega, A. I.: Land
912 surface temperature changes in Northern Iberia since 4000yrBP, based on δ13C of
913 speleothems, Global and Planetary Change, 77, 1–12,
914 https://doi.org/10.1016/j.gloplacha.2011.02.002, 2011.

915   Martín-Puertas, C., Valero-Garcés, B. L., Brauer, A., Mata, M. P., Delgado-Huertas, A., and
916   Dulski, P.: The Iberian-Roman Humid Period (2600-1600 cal yr BP) in the Zoñar Lake varve
917   record (Andalucía, southern Spain), Quaternary Research, 71, 108–120, 2009.

918   Martin-Puertas, C., Matthes, K., Brauer, A., Muscheler, R., Hansen, F., Petrick, C., Aldahan, A.,
919   Possnert, G., and van Geel, B.: Regional atmospheric circulation shifts induced by a grand solar
920   minimum, Nature Geoscience, https://doi.org/10.1038/ngeo1460, 2012.

921   McCormick, M., Büntgen, U., Cane, M. A., Cook, E. R., Harper, K., Huybers, P., Litt, T., Manning,
922   S. W., Mayewski, P. A., More, A. F. M., Nicolussi, K., and Tegel, W.: Climate Change during and
923   after the Roman Empire: Reconstructing the Past from Scientific and Historical Evidence, The
924   Journal of Interdisciplinary History, 43, 169–220, https://doi.org/10.1162/JINH_a_00379, 2012.

925   Morellón, M., Valero-Garcés, B., Vegas-Vilarrúbia, T., González-Sampériz, P., Romero, Ó.,
926   Delgado-Huertas, A., Mata, P., Moreno, A., Rico, M., and Corella, J. P.: Lateglacial and Holocene
927   palaeohydrology in the western Mediterranean region: The Lake Estanya record (NE Spain),
928   Quaternary Science Reviews, 28, 2582–2599, 2009.

929   Morellón, M., Valero-Garcés, B., González-Sampériz, P., Vegas-Vilarrúbia, T., Rubio, E.,
930   Rieradevall, M., Delgado-Huertas, A., Mata, P., Romero, Ó., Engstrom, D. R., López-Vicente, M.,
931   Navas, A., and Soto, J.: Climate changes and human activities recorded in the sediments of
932   Lake Estanya (NE Spain) during the Medieval Warm Period and Little Ice Age, Journal of
933   Paleolimnology, 46, 423–452, https://doi.org/10.1007/s10933-009-9346-3, 2011.

934   Morellón, M., Pérez-Sanz, A., Corella, J. P., Büntgen, U., Catalán, J., González-Sampériz, P.,
935   González-Trueba, J. J., López-Sáez, J. A., Moreno, A., Pla-Rabes, S., Saz-Sánchez, M. Á.,
936   Scussolini, P., Serrano, E., Steinhilber, F., Stefanova, V., Vegas-Vilarrúbia, T., and Valero-Garcés,
937   B.: A multi-proxy perspective on millennium-long climate variability in the Southern Pyrenees,
938   Clim. Past, 8, 683–700, https://doi.org/10.5194/cp-8-683-2012, 2012.

939   Moreno, A., Stoll, H. M., Jiménez-Sánchez, M., Cacho, I., Valero-Garcés, B., Ito, E., and Edwards,
940   L. R.: A speleothem record of rapid climatic shifts during last glacial period from Northern
941   Iberian Peninsula, Global and Planetary Change, 71, 218–231;
942   doi:10.1016/j.gloplacha.2009.10.002, 2010.

943   Moreno, A., Pérez, A., Frigola, J., Nieto-Moreno, V., Rodrigo-Gámiz, M., Martrat, B., González-
944   Sampériz, P., Morellón, M., Martín-Puertas, C., Corella, J. P., Belmonte, Á., Sancho, C., Cacho, I.,
945   Herrera, G., Canals, M., Grimalt, J. O., Jiménez-Espejo, F., Martínez-Ruiz, F., Vegas-Vilarrúbia,
946   T., and Valero-Garcés, B. L.: The Medieval Climate Anomaly in the Iberian Peninsula
947   reconstructed from marine and lake records, Quaternary Science Reviews, 43, 16–32,
948   https://doi.org/10.1016/j.quascirev.2012.04.007, 2012.

949   Moreno, A., Sancho, C., Bartolomé, M., Oliva-Urcia, B., Delgado-Huertas, A., Estrela, M. J.,
950   Corell, D., López-Moreno, J. I., and Cacho, I.: Climate controls on rainfall isotopes and their
951   effects on cave drip water and speleothem growth: the case of Molinos cave (Teruel, NE
952   Spain), Clim Dyn, 43, 221–241, https://doi.org/10.1007/s00382-014-2140-6, 2014.

953   Moreno, A., Pérez-Mejías, C., Bartolomé, M., Sancho, C., Cacho, I., Stoll, H., Delgado-Huertas,
954   A., Hellstrom, J., Edwards, R. L., and Cheng, H.: New speleothem data from Molinos and Ejulve
955   caves reveal Holocene hydrological variability in northeast Iberia, Quaternary Research, 1–11,
956   https://doi.org/10.1017/qua.2017.39, 2017.

957 Moreno, A., Iglesias, M., Azorin-Molina, C., Pérez-Mejías, C., Bartolomé, M., Sancho, C., Stoll,
958 H., Cacho, I., Frigola, J., Osácar, C., Muñoz, A., Delgado-Huertas, A., Blade, I., and Vimeux, F.:
959 Spatial variability of northern Iberian rainfall stable isotope values: Investigating climatic
960 controls on daily and monthly timescales, Atmospheric Chemistry and Physics Discussions, 1–
961 34, https://doi.org/10.5194/acp-2020-861, 2021a.

962 Moreno, A., Bartolomé, M., López-Moreno, J. I., Pey, J., Corella, J. P., García-Orellana, J.,
963 Sancho, C., Leunda, M., Gil-Romera, G., González-Sampériz, P., Pérez-Mejías, C., Navarro, F.,
964 Otero-García, J., Lapazaran, J., Alonso-González, E., Cid, C., López-Martínez, J., Oliva-Urcia, B.,
965 Faria, S. H., Sierra, M. J., Millán, R., Querol, X., Alastuey, A., and García-Ruíz, J. M.: The case of a
966 southern European glacier which survived Roman and medieval warm periods but is
967 disappearing under recent warming, The Cryosphere, 15, 1157–1172,
968 https://doi.org/10.5194/tc-15-1157-2021, 2021b.

969 Morice, C. P., Kennedy, J. J., Rayner, N. A., Winn, J. P., Hogan, E., Killick, R. E., Dunn, R. J. H.,
970 Osborn, T. J., Jones, P. D., and Simpson, I. R.: An Updated Assessment of Near-Surface
971 Temperature Change From 1850: The HadCRUT5 Data Set, Journal of Geophysical Research:
972 Atmospheres, 126, e2019JD032361, https://doi.org/10.1029/2019JD032361, 2021.

973 Naumann, G., Cammalleri, C., Mentaschi, L., and Feyen, L.: Increased economic drought
974 impacts in Europe with anthropogenic warming, Nat. Clim. Chang., 11, 485–491,
975 https://doi.org/10.1038/s41558-021-01044-3, 2021.

976 Neukom, R., Steiger, N., Gómez-Navarro, J. J., Wang, J., and Werner, J. P.: No evidence for
977 globally coherent warm and cold periods over the preindustrial Common Era, Nature, 571,
978 550–554, https://doi.org/10.1038/s41586-019-1401-2, 2019.

979 Observatorio Pirenaico de Cambio Global: Executive summary report OPCC2: Climate change in
980 the Pyrenees:impacts, vulnerability and adaptation, 2018.

981 Oliva, M., Ruiz-Fernández, J., Barriendos, M., Benito, G., Cuadrat, J. M., Domínguez-Castro, F.,
982 García-Ruiz, J. M., Giralt, S., Gómez-Ortiz, A., Hernández, A., López-Costas, O., López-Moreno,
983 J. I., López-Sáez, J. A., Martínez-Cortizas, A., Moreno, A., Prohom, M., Saz, M. A., Serrano, E.,
984 Tejedor, E., Trigo, R., Valero-Garcés, B., and Vicente-Serrano, S. M.: The Little Ice Age in Iberian
985 mountains, Earth-Science Reviews, 177, 175–208,
986 https://doi.org/10.1016/j.earscirev.2017.11.010, 2018.

987 Ortega, P., Lehner, F., Swingedouw, D., Masson-Delmotte, V., Raible, C. C., Casado, M., and
988 Yiou, P.: A model-tested North Atlantic Oscillation reconstruction for the past millennium,
989 Nature, 523, 71–74, https://doi.org/10.1038/nature14518, 2015.

990 PAGES 2k Consortium: Continental-scale temperature variability during the past two millennia,
991 Nature Geosci, 6, 339–346, https://doi.org/10.1038/ngeo1797, 2013.

992 PAGES Hydro2k Consortium: Comparing proxy and model estimates of hydroclimate variability
993 and change over the Common Era, Climate of the Past, 13, 1851–1900,
994 https://doi.org/10.5194/cp-13-1851-2017, 2017.

995 PAGES2k Consortium, Emile-Geay, J., McKay, N. P., Kaufman, D. S., Gunten, L. von, Wang, J.,
996 Anchukaitis, K. J., Abram, N. J., Addison, J. A., Curran, M. A. J., Evans, M. N., Henley, B. J., Hao,
997 Z., Martrat, B., McGregor, H. V., Neukom, R., Pederson, G. T., Stenni, B., Thirumalai, K.,
998 Werner, J. P., Xu, C., Divine, D. V., Dixon, B. C., Gergis, J., Mundo, I. A., Nakatsuka, T., Phipps, S.
999 J., Routson, C. C., Steig, E. J., Tierney, J. E., Tyler, J. J., Allen, K. J., Bertler, N. A. N., Björklund, J.,

Chase, B. M., Chen, M.-T., Cook, E., Jong, R. de, DeLong, K. L., Dixon, D. A., Ekaykin, A. A., Ersek, V., Filipsson, H. L., Francus, P., Freund, M. B., Frezzotti, M., Gaire, N. P., Gajewski, K., Ge, Q., Goosse, H., Gornostaeva, A., Grosjean, M., Horiuchi, K., Hormes, A., Husum, K., Isaksson, E., Kandasamy, S., Kawamura, K., Kilbourne, K. H., Koç, N., Leduc, G., Linderholm, H. W., Lorrey, A. M., Mikhalenko, V., Mortyn, P. G., Motoyama, H., Moy, A. D., Mulvaney, R., Munz, P. M., Nash, D. J., Oerter, H., Opel, T., Orsi, A. J., Ovchinnikov, D. V., Porter, T. J., Roop, H. A., Saenger, C., Sano, M., Sauchyn, D., Saunders, K. M., Seidenkrantz, M.-S., Severi, M., Shao, X., Sicre, M.-A., Sigl, M., Sinclair, K., George, S. S., Jacques, J.-M. S., Thamban, M., Thapa, U. K., Thomas, E. R., Turney, C., Uemura, R., Viau, A. E., Vladimirova, D. O., Wahl, E. R., White, J. W. C., Yu, Z., and Zinke, J.: A global multiproxy database for temperature reconstructions of the Common Era, Scientific Data, 4, sdata201788, https://doi.org/10.1038/sdata.2017.88, 2017.

Peregrine, P. N.: Climate and social change at the start of the Late Antique Little Ice Age, The Holocene, 30, 1643–1648, https://doi.org/10.1177/0959683620941079, 2020.

Pérez-Mejías, C., Moreno, A., Sancho, C., Bartolomé, M., Stoll, H., Osácar, M. C., Cacho, I., and Delgado-Huertas, A.: Transference of isotopic signal from rainfall to dripwaters and farmed calcite in Mediterranean semi-arid karst, Geochimica et Cosmochimica Acta, 243, 66–98, https://doi.org/10.1016/j.gca.2018.09.014, 2018.

Pérez-Zanón, N., Sigró, J., and Ashcroft, L.: Temperature and precipitation regional climate series over the central Pyrenees during 1910–2013, International Journal of Climatology, 37, 1922–1937, https://doi.org/10.1002/joc.4823, 2017.

Pla, S. and Catalan, J.: Chrysophyte cysts from lake sediments reveal the submillennial winter/spring climate variability in the northwestern Mediterranean region throughout the Holocene, Climate Dynamics, 24, 263–278, https://doi.org/10.1007/s00382-004-0482-1, 2005.

Pla-Rabes, S. and Catalan, J.: Deciphering chrysophyte responses to climate seasonality, J Paleolimnol, 46, 139, https://doi.org/10.1007/s10933-011-9529-6, 2011.

Priestley, S. C., Treble, P. C., Griffiths, A. D., Baker, A., Abram, N. J., and Meredith, K. T.: Caves demonstrate decrease in rainfall recharge of southwest Australian groundwater is unprecedented for the last 800 years, Commun Earth Environ, 4, 1–12, https://doi.org/10.1038/s43247-023-00858-7, 2023.

Reimer, P.: Discussion: Reporting and Calibration of Post-Bomb 14C Data, Radiocarbon, 46, 1299–1304, https://doi.org/10.1017/S0033822200033154, 2004.

Rico, I., Izagirre, E., Serrano, E., and López-Moreno, J. I.: Superficie glaciar actual en los Pirineos: Una actualización para 2016, Pirineos, 172, 029, https://doi.org/10.3989/Pirineos.2017.172004, 2017.

Sánchez-López, G., Hernández, A., Pla-Rabes, S., Trigo, R. M., Toro, M., Granados, I., Sáez, A., Masqué, P., Pueyo, J. J., Rubio-Inglés, M. J., and Giralt, S.: Climate reconstruction for the last two millennia in central Iberia: The role of East Atlantic (EA), North Atlantic Oscillation (NAO) and their interplay over the Iberian Peninsula, Quaternary Science Reviews, 149, 135–150, https://doi.org/10.1016/j.quascirev.2016.07.021, 2016.

Sancho, C., Belmonte, Á., Bartolomé, M., Moreno, A., Leunda, M., and López-Martínez, J.: Middle-to-late Holocene palaeoenvironmental reconstruction from the A294 ice-cave record (Central Pyrenees, northern Spain), Earth and Planetary Science Letters, 484, 135–144, https://doi.org/10.1016/j.epsl.2017.12.027, 2018.

1043   Scholz, D. and Hoffmann, D. L.: StalAge - An algorithm designed for construction of speleothem
1044   age models, Quaternary Geochronology, 6, 369–382,
1045   https://doi.org/10.1016/j.quageo.2011.02.002, 2011.

1046   Schurer, A. P., Tett, S. F. B., and Hegerl, G. C.: Small influence of solar variability on climate
1047   over the past millennium, Nature Geosci, 7, 104–108, https://doi.org/10.1038/ngeo2040,
1048   2014.

1049   Shen, C. C., Edwards, R. L., Cheng, H., Dorale, J. A., Thomas, R. B., Moran, S. B., Weinstein, S. E.,
1050   and Edmonds, H. N.: Uranium and thorium isotopic and concentration measurements by
1051   magnetic sector inductively coupled plasma mass spectrometry, Chemical Geology, 185, 165–
1052   178, 2002.

1053   Shindell, D. T., Schmidt, G. A., Mann, M. E., Rind, D., and Waple, A.: benito, Science, 294, 2149,
1054   2001.

1055   Sigl, M., Winstrup, M., McConnell, J. R., Welten, K. C., Plunkett, G., Ludlow, F., Büntgen, U.,
1056   Caffee, M., Chellman, N., Dahl-Jensen, D., Fischer, H., Kipfstuhl, S., Kostick, C., Maselli, O. J.,
1057   Mekhaldi, F., Mulvaney, R., Muscheler, R., Pasteris, D. R., Pilcher, J. R., Salzer, M., Schüpbach,
1058   S., Steffensen, J. P., Vinther, B. M., and Woodruff, T. E.: Timing and climate forcing of volcanic
1059   eruptions for the past 2,500 years, Nature, 523, 543–549,
1060   https://doi.org/10.1038/nature14565, 2015.

1061   Spötl, C.: Long-term performance of the Gasbench isotope ratio mass spectrometry system for
1062   the stable isotope analysis of carbonate microsamples, Rapid Commun. Mass Spectrom., 25,
1063   1683–1685, https://doi.org/10.1002/rcm.5037, 2011.

1064   Steffen, W., Broadgate, W., Deutsch, L., Gaffney, O., and Ludwig, C.: The trajectory of the
1065   Anthropocene: The Great Acceleration, The Anthropocene Review, 2, 81–98,
1066   https://doi.org/10.1177/2053019614564785, 2015.

1067   Sundqvist, H. S., Holmgren, K., Moberg, A., Spötl, C., and Mangini, A.: Stable isotopes in a
1068   stalagmite from NW Sweden document environmental changes over the past 4000 years,
1069   Boreas, 39, 77–86, https://doi.org/10.1111/j.1502-3885.2009.00099.x, 2010.

1070   Swingedouw, D., Terray, L., Cassou, C., Voldoire, A., Salas-Melia, D., and Servonnat, J.: Natural
1071   forcing of climate during the last millennium: fingerprint of solar variability, Climate Dynamics,
1072   36, 1349–1364, https://doi.org/10.1007/s00382-010-0803-5, 2011.

1073   Tadros, C. V., Markowska, M., Treble, P. C., Baker, A., Frisia, S., Adler, L., and Drysdale, R. N.:
1074   Recharge variability in Australia's southeast alpine region derived from cave monitoring and
1075   modern stalagmite δ18O records, Quaternary Science Reviews, 295, 107742,
1076   https://doi.org/10.1016/j.quascirev.2022.107742, 2022.

1077   Thatcher, D. L., Wanamaker, A. D., Denniston, R. F., Ummenhofer, C. C., Asmerom, Y., Polyak,
1078   V. J., Cresswell-Clay, N., Hasiuk, F., Haws, J., and Gillikin, D. P.: Iberian hydroclimate variability
1079   and the Azores High during the last 1200 years: evidence from proxy records and climate
1080   model simulations, Clim Dyn, https://doi.org/10.1007/s00382-022-06427-6, 2022.

1081   Trachsel, M., Kamenik, C., Grosjean, M., McCarroll, D., Moberg, A., Brázdil, R., Büntgen, U.,
1082   Dobrovolný, P., Esper, J., Frank, D. C., Friedrich, M., Glaser, R., Larocque-Tobler, I., Nicolussi, K.,
1083   and Riemann, D.: Multi-archive summer temperature reconstruction for the European Alps,

1084   AD 1053–1996, Quaternary Science Reviews, 46, 66–79,
1085   https://doi.org/10.1016/j.quascirev.2012.04.021, 2012.

1086   Treble, P. C., Baker, A., Abram, N. J., Hellstrom, J. C., Crawford, J., Gagan, M. K., Borsato, A.,
1087   Griffiths, A. D., Bajo, P., Markowska, M., Priestley, S. C., Hankin, S., and Paterson, D.:
1088   Ubiquitous karst hydrological control on speleothem oxygen isotope variability in a global
1089   study, Commun Earth Environ, 3, 1–10, https://doi.org/10.1038/s43247-022-00347-3, 2022.

1090   Tremaine, D. M., Froelich, P. N., and Wang, Y.: Speleothem calcite farmed in situ: Modern
1091   calibration of δ18O and δ13C paleoclimate proxies in a continuously-monitored natural cave
1092   system, Geochimica et Cosmochimica Acta, 75, 4929–4950,
1093   https://doi.org/10.1016/j.gca.2011.06.005, 2011.

1094   Trouet, V., Esper, J., Graham, N. E., Baker, A., Scourse, J. D., and Frank, D. C.: Persistent Positive
1095   North Atlantic Oscillation Mode Dominated the Medieval Climate Anomaly, Science, 324, 78–
1096   80, 2009.

1097   Trouet, V., Scourse, J. D., and Raible, C. C.: North Atlantic storminess and Atlantic Meridional
1098   Overturning Circulation during the last Millennium: Reconciling contradictory proxy records of
1099   NAO variability, Global and Planetary Change, 84–85, 48–55,
1100   https://doi.org/10.1016/j.gloplacha.2011.10.003, 2012.

1101   Usoskin, I. G., Hulot, G., Gallet, Y., Roth, R., Licht, A., Joos, F., Kovaltsov, G. A., Thébault, E., and
1102   Khokhlov, A.: Evidence for distinct modes of solar activity, A&A, 562, L10,
1103   https://doi.org/10.1051/0004-6361/201423391, 2014.

1104   Usoskin, I. G., Gallet, Y., Lopes, F., Kovaltsov, G. A., and Hulot, G.: Solar activity during the
1105   Holocene: the Hallstatt cycle and its consequence for grand minima and maxima, A&A, 587,
1106   A150, https://doi.org/10.1051/0004-6361/201527295, 2016.

1107   Vegas-Vilarrúbia, T., Corella, J. P., Sigró, J., Rull, V., Dorado-Liñan, I., Valero-Garcés, B., and
1108   Gutiérrez-Merino, E.: Regional precipitation trends since 1500 CE reconstructed from calcite
1109   sublayers of a varved Mediterranean lake record (Central Pyrenees), Science of The Total
1110   Environment, 826, 153773, https://doi.org/10.1016/j.scitotenv.2022.153773, 2022.

1111   Vicente de Vera García, A., Mata-Campo, M. P., Pla, S., Vicente, E., Prego, R., Frugone-Álvarez,
1112   M., Polanco-Martínez, J., Galofré, M., and Valero-Garcés, B. L.: Unprecedented recent regional
1113   increase in organic carbon and lithogenic fluxes in high altitude Pyrenean lakes, Sci Rep, 13,
1114   8586, https://doi.org/10.1038/s41598-023-35233-1, 2023.

1115   Vidaller, I., Revuelto, J., Izagirre, E., Rojas-Heredia, F., Alonso-González, E., Gascoin, S., René, P.,
1116   Berthier, E., Rico, I., Moreno, A., Serrano, E., Serreta, A., and López-Moreno, J. I.: Toward an
1117   Ice-Free Mountain Range: Demise of Pyrenean Glaciers During 2011–2020, Geophys Res Lett,
1118   48, https://doi.org/10.1029/2021GL094339, 2021.

1119   Welte, C., Wacker, L., Hattendorf, B., Christl, M., Koch, J., Synal, H.-A., and Günther, D.: Novel
1120   Laser Ablation Sampling Device for the Rapid Radiocarbon Analysis of Carbonate Samples by
1121   Accelerator Mass Spectrometry, Radiocarbon, 58, 419–435,
1122   https://doi.org/10.1017/RDC.2016.6, 2016.

1123   Zawiska, I., Luoto, T. P., Nevalainen, L., Tylmann, W., Jensen, T. C., Obremska, M., Słowiński,
1124   M., Woszczyk, M., Schartau, A. K., and Walseng, B.: Climate variability and lake ecosystem
1125   responses in western Scandinavia (Norway) during the last Millennium, Palaeogeography,

1126   Palaeoclimatology, Palaeoecology, 466, 231–239,
1127   https://doi.org/10.1016/j.palaeo.2016.11.034, 2017.

1128

 Figure captions

 Figure 1. a) Location of regional speleothem records covering last 2500 years to be compared with the
 samples studied in the Pyrenees (red rectangle, enlarged in Fig. 1B). b) Location of caves (orange circles)
 and other nearby records from northern Spain. See legend for the different types of available paleoclimate
 archives. c) Location of the four studied caves in the Central Pyrenees of NE Spain in the vicinity of the
 Ordesa and Monte Perdido National Park. Source base map: digital elevation model and hillshade derived
 from Mapzen Global Terrain, coastline, boundaries and geographic lines from NaturalEarthData.com
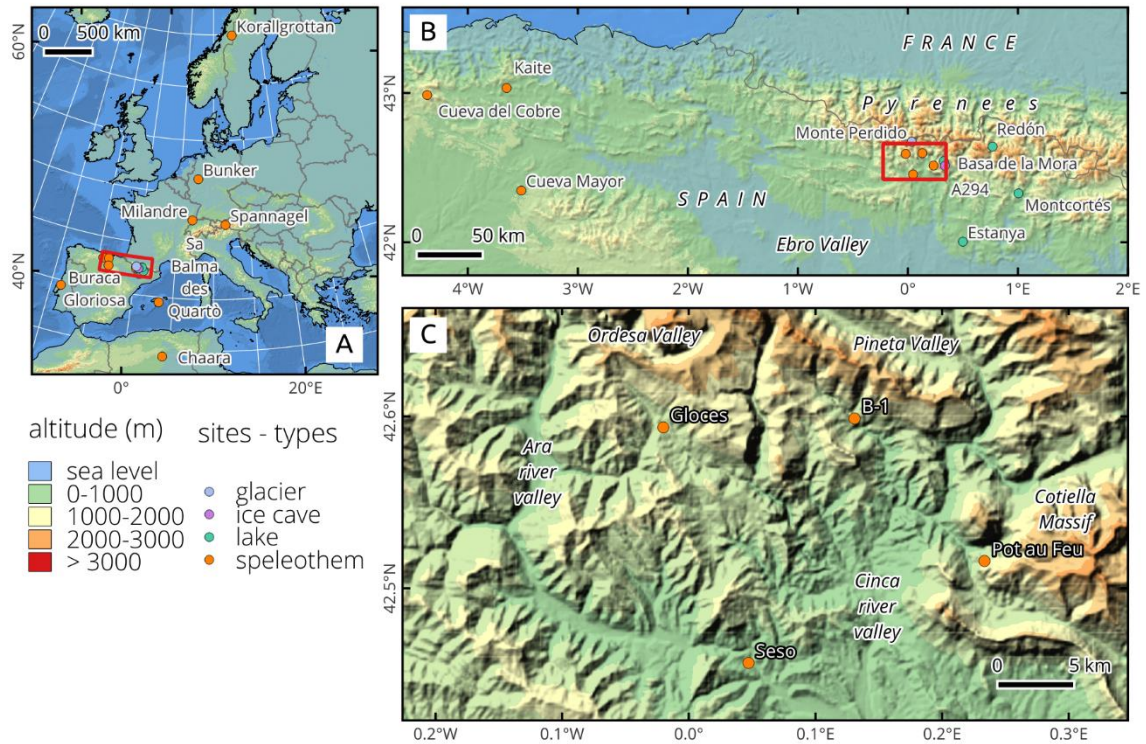
1136

1137

1138 **Figure 2**. [14]C activity (expressed as F[14]C, following recommendations made in Reimer, 2004) of the top
1139 parts of stalagmites MIC (a) and XEV (b) from Seso Cave. The start of the increase in F[14]C and its
1140 maximum are recorded at 1955 and 1963 CE, respectively, in both stalagmites. c) Composite δ^{18}O record
1141 using *Iscam* with data from MIC and XEV stalagmites.
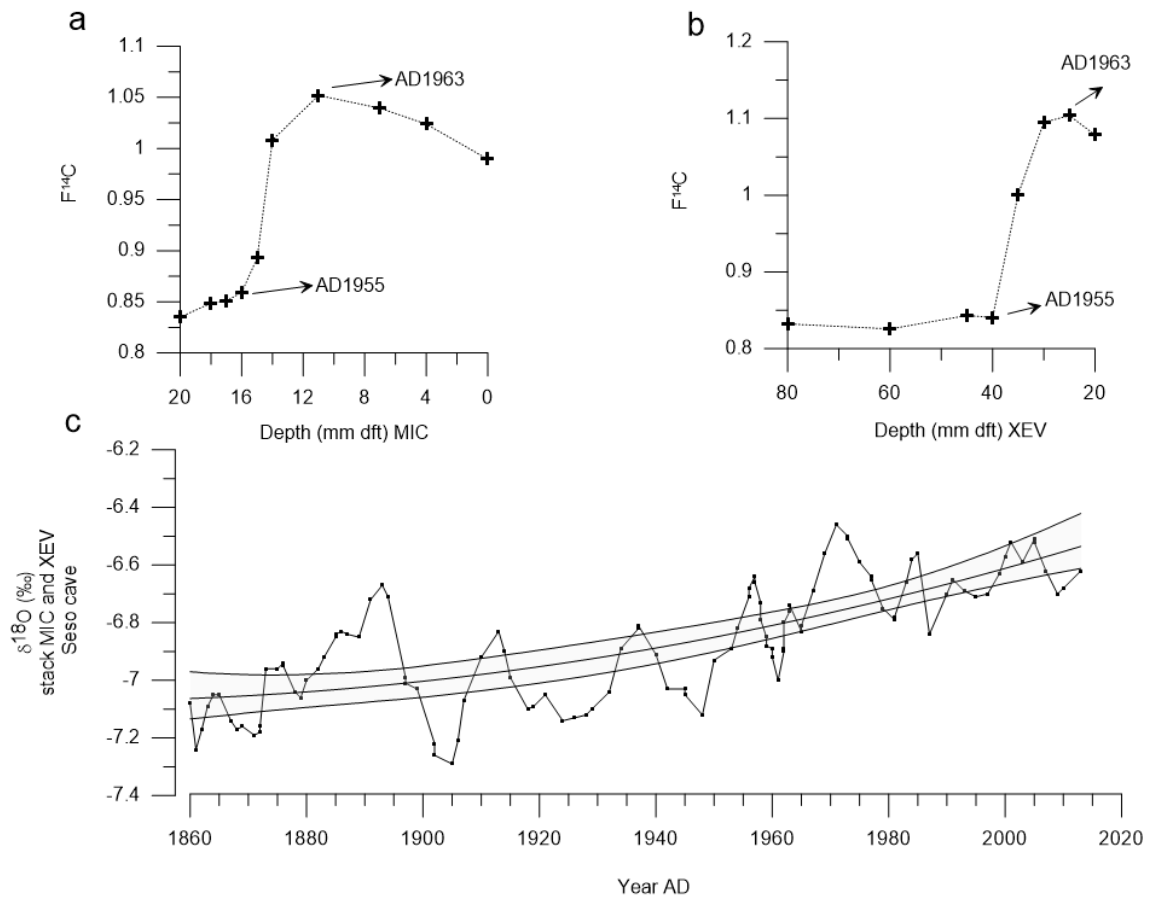
1142

1143

1144 **Figure 3**. Comparison of individual δ¹⁸O records from four Pyrenean caves, (a) Seso; (b) Pot au Feu; (c)
1145 B1 and (d) Las Gloces caves, and (e) the composite δ¹⁸O record produced using *Iscam* (black curve) for the
1146 last 2500 years. Generating Seso and Las Gloces curves required *Iscam* age modelling while Pot au Feu
1147 and B1 curves represent only one stalagmite, which age model was produced by StalAge modelling. Black
1148 double arrows indicate intervals with patterns present in all records. MCA: Medieval Climate Anomaly,
1149 IE: Industrial Era.
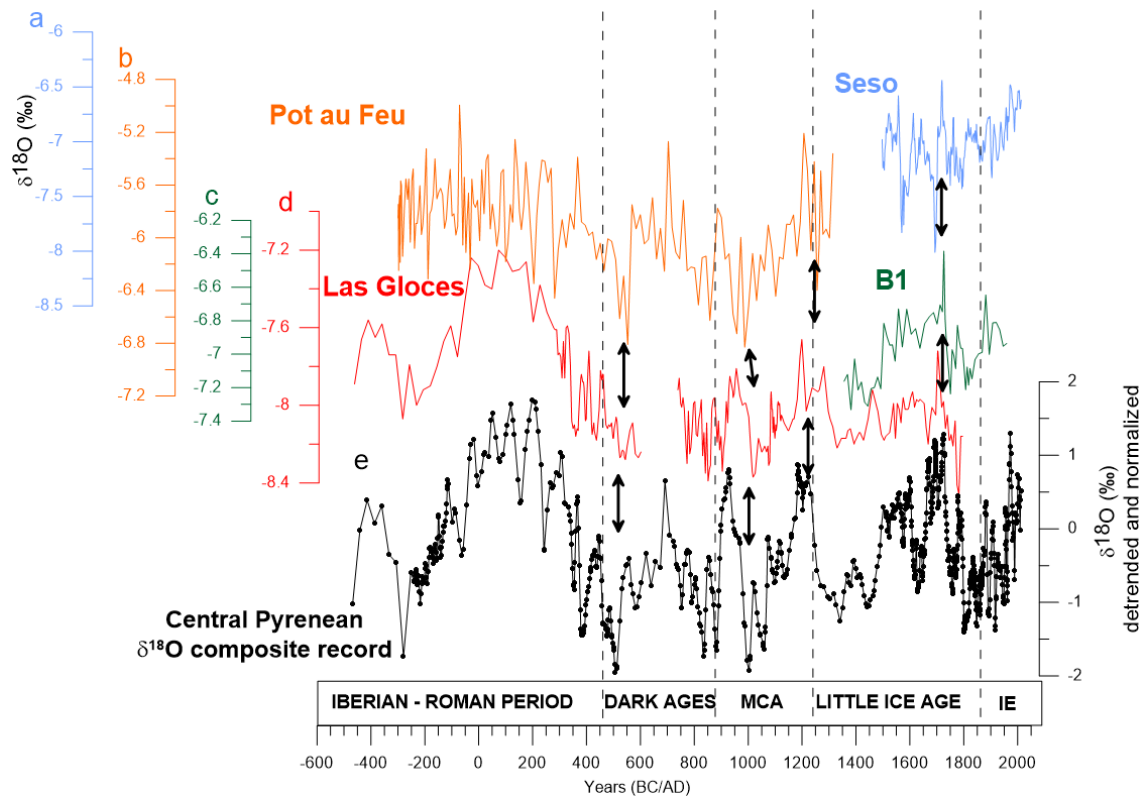
1150

1151

Figure 4. a) Central Pyrenean δ¹⁸O composite record for the last 2500 years based on eight stalagmites from four caves. Blue bars mark intervals of δ¹⁸O values below -0.75, while yellow bars mark those with δ¹⁸O values above +0.75 (note this composite record was obtained from normalized records, so it varies among – 3 and 3 without possibility of direct translation to absolute δ¹⁸O values). b) Rainfall reconstructed from calcite layers from Montcortés lake in the Pre-Pyrenees (Corella et al., 2016). c) Salinity reconstructed from geochemical data from Estanya lake in the Pre-Pyrenees (González-Sampériz et al., 2017; Morellón et al., 2012, 2011). d) Snow and ice accumulation in ice cave A294 in the Cotiella massif of the Central Pyrenees (Sancho et al., 2018), and e) Pyrenean temperature reconstruction based on tree-ring data (Büntgen et al., 2017). MCA: Medieval Climate Anomaly, IE: Industrial Era.
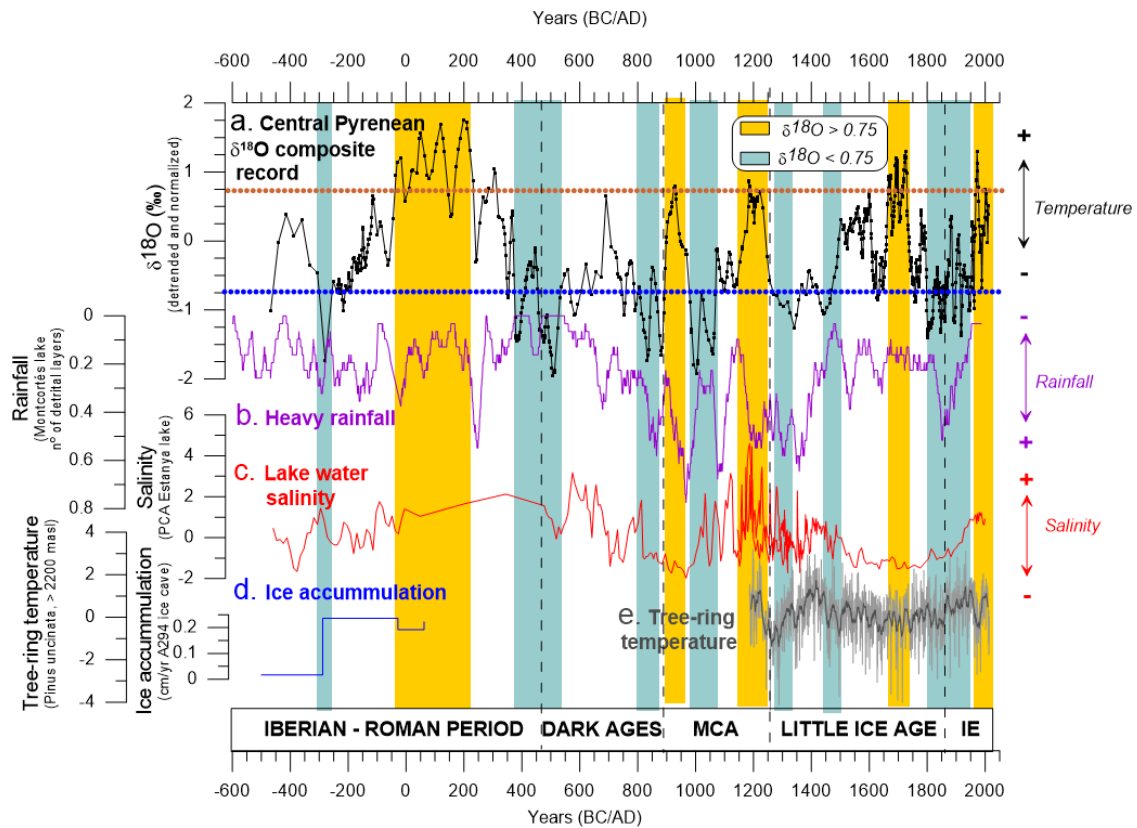
Figure 5. Comparison of European and W Mediterranean speleothem records covering the last 2500 years. a) winter NAO reconstruction based on growth rate of Irish speleothems (Baker et al., 2015); b) precipitation variability reconstructed for W Portugal (Thatcher et al., 2022), c) Balearic Islands (Cisneros et al., 2021), and d) Morocco (Ait Brahim et al., 2019); temperature variation reconstructed from e) Sweden (Sundqvist et al., 2010), f) Central Europe (Affolter et al., 2019; Fohlmeister et al., 2012), g) Alps (Mangini et al., 2005) and h) Northern Iberia (Martín-Chivelet et al., 2011); i) Central Pyrenean δ^{18}O composite record (this study). Black arrows indicate intervals of well-reproduced patterns during the Dark Ages and the Little Ice Age cold intervals. MCA: Medieval Climate Anomaly, IE: Industrial Era.
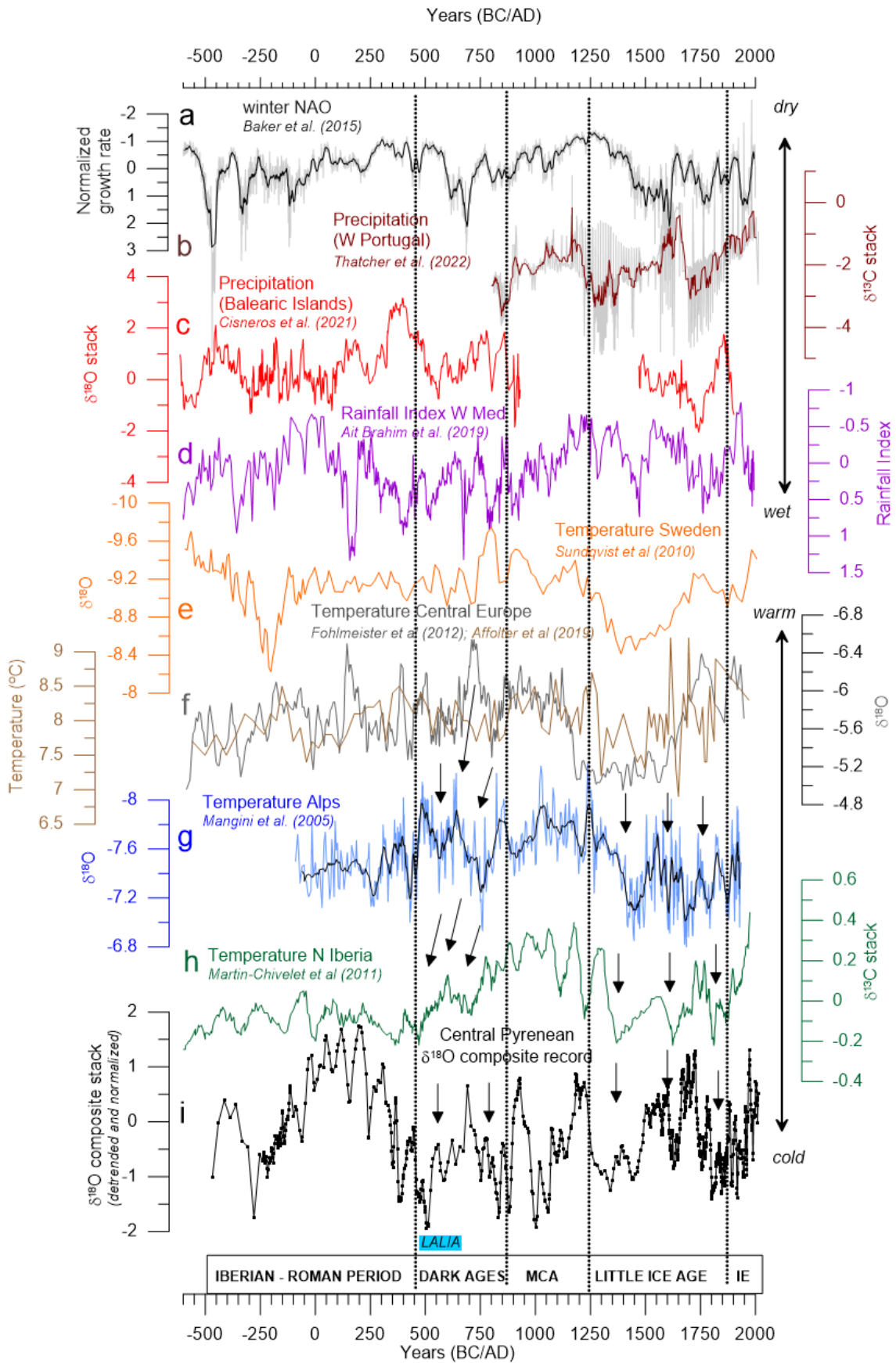
1171

1172

Figure 6. Global records and forcing mechanisms. a) volcanic forcing represented by the (nss)S (ppb) in the NEEM ice core (blue line); b) changes in the irradiance as a consequence of Northern Hemisphere volcanic eruptions (Sigl et al., 2015) (brown bars); c) sunspot numbers (Usoskin et al., 2014); d) probability of paleofloods in European temperate regions (Benito et al., 2015); e) worldwide tree-ring compilation (green line, running average width window = 15) (Sigl et al., 2015); f) temperature reconstruction from Europe, compiled by the PAGES2k group (red line, running average width window = 15) (PAGES 2k Consortium, 2013); g) the NAO reconstruction for the Central Iberian Peninsula (purple line) and the 95% (light grey band) uncertainty intervals and h) Central Pyrenean δ18O composite record (this study). Light brown bars indicate warming periods during the Roman Period, the end of the MCA and in recent decades. Light blue bands mark cooling events during the DA while dark blue bands mark solar minima (Oort, Wolf, Spörer, Maunder and Dalton). MCA: Medieval Climate Anomaly, IE: Industrial Era.
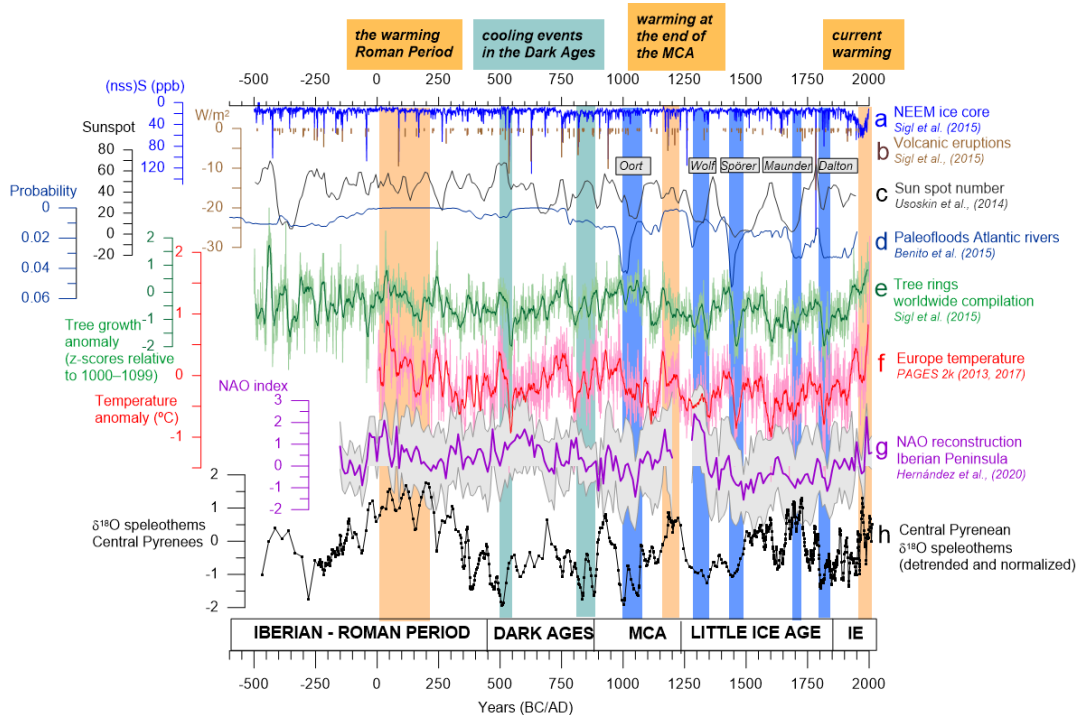
1186 **Table 1**. Sample characteristics

Cave	Sample ID	Length (cm)	Number of U-Th dates (used in StalAge)	Interval covered (years BCE/CE in StalAge)	Sampling resolution (average years per isotope sample)	Comments
Seso	MIC	8.5	8	1718-2010 CE	3.8 years	Growth to present
	XEV	26	9	1501-2013 CE	1.9 years	Two growth periods, no hiatus. Growth to present
	CHA	8.5	3	1573-1779 CE	3.5 years	The uppermost 7 mm are not sampled
	CLA	10.5 (a hiatus at 8.5 cm)	4	1826-1935 CE	1.5 years	The uppermost 2 cm are not sampled
Las Gloces	ISA	13.5 (a hiatus at 7 cm)	7	346-607 CE 845-634 CE	11.4 years	In StalAge, one date is not included due to high error
	LUC	23.3 (a hiatus at 12.5 cm)	6	471BCE-504 CE 547-1991 CE	11.2 years	Really short hiatus
B-1	TAR	7.5 cm	8	1355-1959 CE	10.5 years	
Pot au Feu	JAR	80 cm	10	299BCE-1314 CE	10 years	

1187
1188

1189
1190 **Table 2.** [230]Th dating results of the eight stalagmites examined in this study (data from the University of
1191 Minnesota, University of Xi'an and University of Melbourne). Analytical errors are 2σ of the mean. The
1192 sample marked by a red asterisk was discarded due to the high error.
1193

Sample ID	^{238}U (ppb)	^{232}Th (ppt)	^{230}Th/^{232}Th (b) (atomic x10^{-6})	δ^{234}U (*) (measured)	^{230}Th/^{238}U (a) (activity)	^{230}Th Age (yr) (uncorrected)	^{230}Th Age (yr) (corrected)	δ^{234}U$_{init}$ (**) (corrected)	^{230}Th Age (yr BP) (***) (corrected)
Seso cave									
Xer-0	451 ±1	12292 ±248	4.0 ±0.1	454.3 ±3.1	0.0066 ±0.0001	495 ±8	-52 ±387	454 ±3	-115 ±387
Xer-55	355 ±1	2875 ±58	4.2 ±0.2	434.3 ±2.9	0.0021 ±0.0001	159 ±8	-6 ±116	434 ±3	-69 ±116
Xer-85	299 ±1	1557 ±31	8 ±0	424.6 ±3.1	0.0027 ±0.0001	204 ±9	97 ±76	425 ±3	34 ±76
Xer-110	308 ±1	798 ±16	18 ±1	410.5 ±2.4	0.0029 ±0.0001	223 ±9	170 ±39	411 ±2	107 ±39
Xer-145	267 ±1	535 ±11	25 ±1	404.7 ±2.7	0.0030 ±0.0001	236 ±10	195 ±31	405 ±3	132 ±31
Xer-190	261 ±1	340 ±7	54 ±2	419.0 ±2.8	0.0043 ±0.0001	328 ±10	301 ±22	419 ±3	238 ±22
Xer-210	299 ±1	1445 ±29	20 ±1	420.8 ±3.5	0.0059 ±0.0001	452 ±12	353 ±71	421 ±4	290 ±71
Xer-240	277 ±1	1758 ±35	19 ±1	436.4 ±2.7	0.0072 ±0.0002	548 ±12	420 ±92	437 ±3	357 ±92
Xer-280	339 ±1	2459 ±50	20 ±0	414.7 ±3.8	0.0086 ±0.0001	667 ±10	517 ±106	415 ±4	454 ±106
Mic-0	503 ±1	4623 ±93	5 ±0	485.9 ±2.4	0.0027 ±0.0001	196 ±6	16 ±128	486 ±2	-46 ±128
Mic-5	441 ±1	1166 ±23	6 ±1	487.3 ±2.3	0.0009 ±0.0002	69 ±11	17 ±38	487 ±2	-45 ±38
Mic-20	412 ±1	127 ±3	73 ±6	477.0 ±2.3	0.0014 ±0.0001	101 ±8	95 ±9	477 ±2	33 ±9
Mic-35	427 ±1	708 ±14	25 ±1	455.2 ±2.3	0.0025 ±0.0001	191 ±8	158 ±25	455 ±3	96 ±25
Mic-48	417 ±1	603 ±12	34 ±1	455.7 ±3.0	0.0030 ±0.0001	223 ±8	205 ±15	456 ±3	142 ±15
Mic-60	393 ±1	1049 ±21	23 ±1	461.4 ±3.8	0.0037 ±0.0001	274 ±8	242 ±24	462 ±4	179 ±24
Mic-67	413 ±1	3812 ±77	9 ±0	458.7 ±2.9	0.0051 ±0.0001	380 ±8	196 ±130	459 ±3	134 ±130
Mic-75	389 ±1	25715 ±517	4 ±0	458.0 ±2.5	0.0144 ±0.0002	1080 ±15	267 ±576	458 ±3	204 ±576
Cla-0	346 ±1	332 ±7	34 ±2	371.5 ±3.1	0.0026 ±0.0001	158 ±9	138 ±17	372 ±3	75 ±17
Cla-25	368 ±1	493 ±10	32 ±1	367.1 ±2.9	0.0026 ±0.0001	204 ±8	176 ±22	367 ±3	113 ±22
Cla-70	346 ±1	1262 ±25	17 ±1	367.8 ±2.4	0.0037 ±0.0001	298 ±8	221 ±56	368 ±2	158 ±56
Cla-74	319 ±1	226 ±5	70 ±3	368.6 ±2.7	0.0030 ±0.0001	240 ±9	225 ±14	369 ±3	162 ±14
Cha-0	393.0 ±0.7	169 ±3	116 ±6	381.0 ±2.0	0.0030 ±0.0001	239 ±11	230 ±13	381 ±2	168 ±13
Cha-30	342.9 ±1.0	609 ±12	47 ±2	381.0 ±2.0	0.0050 ±0.0001	398 ±12	360 ±29	382 ±2	298 ±29
Cha-58	348.1 ±0.8	396 ±8	84 ±2	387.3 ±2.7	0.0058 ±0.0001	457 ±9	434 ±19	388 ±3	372 ±19
Las Gloces cave									
Isa-0	167.1 ±0.3	451 ±9	233 ±5	1465.3 ±3.4	0.0382 ±0.0003	1700 ±14	1668 ±26	1472 ±3	1605 ±26
Isa-4	119.9 ±0.2	291 ±6	221 ±5	1487.0 ±4.1	0.0325 ±0.0003	1434 ±15	1406 ±25	1493 ±4	1343 ±25
Isa-4.5	115.0 ±0.1	905 ±18	61 ±2	1510.8 ±3.1	0.0289 ±0.0004	1262 ±19	1171 ±67	1516 ±3	1108 ±67
Isa-6	107.7 ±0.2	8522 ±171	5 ±1	1504.8 ±4.5	0.0253 ±0.0004	1107 ±20	185 ±653	1506 ±5	122 ±653 (*)
Isa-8	108.4 ±0.1	261 ±5	142 ±4	1504.6 ±3.6	0.0207 ±0.0004	905 ±17	877 ±26	1508 ±5	814 ±26
Isa-11	69.5 ±0.1	2977 ±60	8 ±1	1505.3 ±3.7	0.0201 ±0.0006	877 ±26	379 ±353	1507 ±4	316 ±353
Luc-0	88 ±1	2350 ±47	56 ±1	1859 ±4	0.0699 ±0.0006	2693 ±23	2483 ±150	1872 ±4	2420 ±150
Luc-5.5	88 ±1	539 ±11	127 ±3	1848 ±4	0.0469 ±0.0005	1806 ±18	1744 ±47	1857 ±4	1681 ±47
Luc 10	131 ±0.2	388 ±8	213 ±5	1721.6 ±3.2	0.0382 ±0.0003	1540 ±16	1508 ±27	1729 ±3.2	1445 ±27
Luc-11	81 ±1	955 ±19	50 ±1	1796 ±5	0.0359 ±0.0006	1407 ±23	1184 ±90	1803 ±5	1211 ±90
Luc-15.5	73 ±0	282 ±6	118 ±3	1783 ±6	0.0279 ±0.0006	1098 ±22	1057 ±36	1789 ±6	994 ±36
Luc-18.5	72 ±0	1477 ±30	16 ±1	1705 ±5	0.0202 ±0.0005	818 ±22	597 ±158	1708 ±5	534 ±158
Luc-22.5	139 ±0	287 ±6	47 ±2	1554 ±3	0.0058 ±0.0002	660 ±4	226 ±20	1555 ±3	163 ±20
B-1 cave									
B1-12.5- 56 mm	6083 ±27	797 ±16	49 ±2	-288.5 ±2.5	0.0039 ±0.0002	59 ±3	54 ±5	-289 ±2	-9 ±5
B1-12.5- 44 mm	6492 ±32	201 ±4	630 ±14	-295.8 ±1.8	0.00119 ±0.00001	184 ±2	182 ±2	-296 ±2	120 ±2
B1-12.5- 37 mm	10036 ±47	616 ±12	392 ±9	-290.2 ±2.3	0.00146 ±0.0001	224 ±2	222 ±3	-290 ±2	159 ±3
B1-12.5- 31 mm	8347 ±31	10930 ±219	2.0 ±1	-295.1 ±1.4	0.00159 ±0.0002	247 ±3	193 ±38	-295 ±1	130 ±38
B1-12.5- 26 mm	7424 ±27	1633 ±33	156 ±3	-294.3 ±1.5	0.00200 ±0.00002	321 ±3	312 ±7	-295 ±2	249 ±7
B1-12.5- 16 mm	8318 ±31	385 ±8	1052 ±23	-295.2 ±2.0	0.00295 ±0.00002	458 ±4	456 ±4	-296 ±2	393 ±4
B1-12.5- 10 mm	9499 ±41	551 ±11	961 ±20	-290.9 ±1.5	0.00338 ±0.00002	521 ±4	519 ±4	-291 ±2	456 ±4
B1-12.5- 0 mm	8128 ±33	649 ±13	884 ±18	-290.2 ±1.9	0.00428 ±0.00002	660 ±4	657 ±5	-291 ±2	594 ±5

U decay constants: λ_{238} = 1.55125x10^{-10} (Jaffey et al., 1971) and λ_{234} = 2.82206x10^{-6} (Cheng et al., 2013). Th decay constant: λ_{230} = 9.1705x10^{-6} (Cheng et al., 2013).

* δ^{234}U = ([^{234}U/^{238}U]$_{activity}$ − 1)x1000.

** δ^{234}U$_{initial}$ was calculated based on ^{230}Th age (T), i.e., δ^{234}U$_{initial}$ = δ^{234}U$_{measured}$ x e$^{\lambda_{234}T}$.

Corrected ^{230}Th ages assume the initial ^{230}Th/^{232}Th atomic ratio of 4.4 ±2.2 x10^{-6}. Those are the values for a material at secular equilibrium, with the bulk earth ^{232}Th/^{238}U value of 3.8. The errors are arbitrarily assumed to be 50%.

*** B.P. stands for "Before Present" where the "Present" is defined as the year 1950 A.D.

1194

1195

		Pot au Feu cave							
Sample	^{238}U (ppb)	$^{230}Th/^{238}U$ (a)	$^{234}U/^{238}U$ (a)	$^{232}Th/^{238}U$ (a)	$^{230}Th/^{232}Th$ (a)	^{230}Th Age (yr) uncorrected	Age (yr BP) (b)	error	$^{234}U/^{238}U$ Initial (c)
CT-PF 7.5	109	0.022	1.570	0.0084	2.6	1508	746	±193	1.572
CT-PF 47	NR	0.013	1.563	0.0017	7.3	884	733	±79	1.565
CT-PF 95	NR	0.014	1.580	0.0015	9.1	956	822	±82	1.581
CT-PF 205	95	0.019	1.565	0.0017	11.0	1330	1176	±68	1.567
CT-PF 335	NR	0.030	1.533	0.0051	5.8	2117	1652	±253	1.536
CT-PF 400	131	0.029	1.533	0.0033	8.6	2041	1739	±140	1.535
CT-PF 510	NR	0.033	1.534	0.0046	7.1	2347	1934	±145	1.537
CT-PF 640	103	0.036	1.600	0.0052	7.1	2503	2060	±146	1.604
CT-PF 740	109	0.022	1.570	0.0084	2.6	1508	2221	±237	1.572
CT-PF 790	NR	0.013	1.563	0.0017	7.3	884	2099	±463	1.565

(a) Activity ratios determined after Hellstrom (2003) using the decay constants of (Cheng et al., 2000)

(b) Age in kyr before present corrected for initial ^{230}Th using eqn. 1 of (Hellstrom, 2006) and [$^{230}Th/^{232}Th$]i of 0.9 ± 0.4

(c) Initial [$^{234}U/^{238}U$] calculated using corrected age

1196
1197
1198
1199

1200

1201 **Appendix A**

1202 **Figure A1.** Polished slabs, age-depth model using StalAge (left) and proxy profiles versus age (right) for
1203 the stalagmites used in this study arranged by cave (a. Seso, b. Las Gloces, c. B1, and d. Pot au Feu caves).
1204 Correlation coefficients among the three proxies are indicated based on Pearson correlation. Horizontal
1205 lines represent the age error for every data point, following StalAge uncertainty.

1206 a- Seso cave
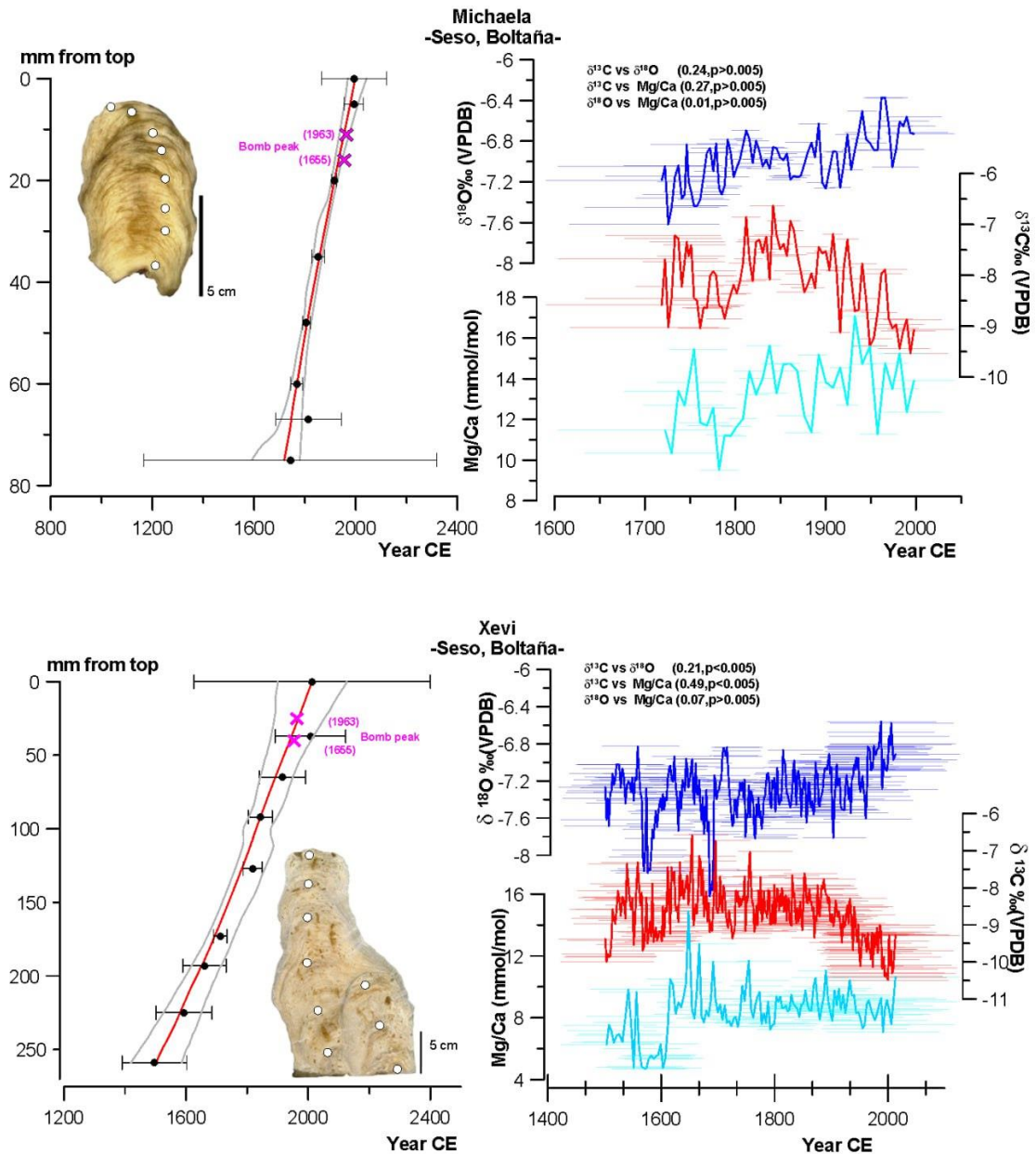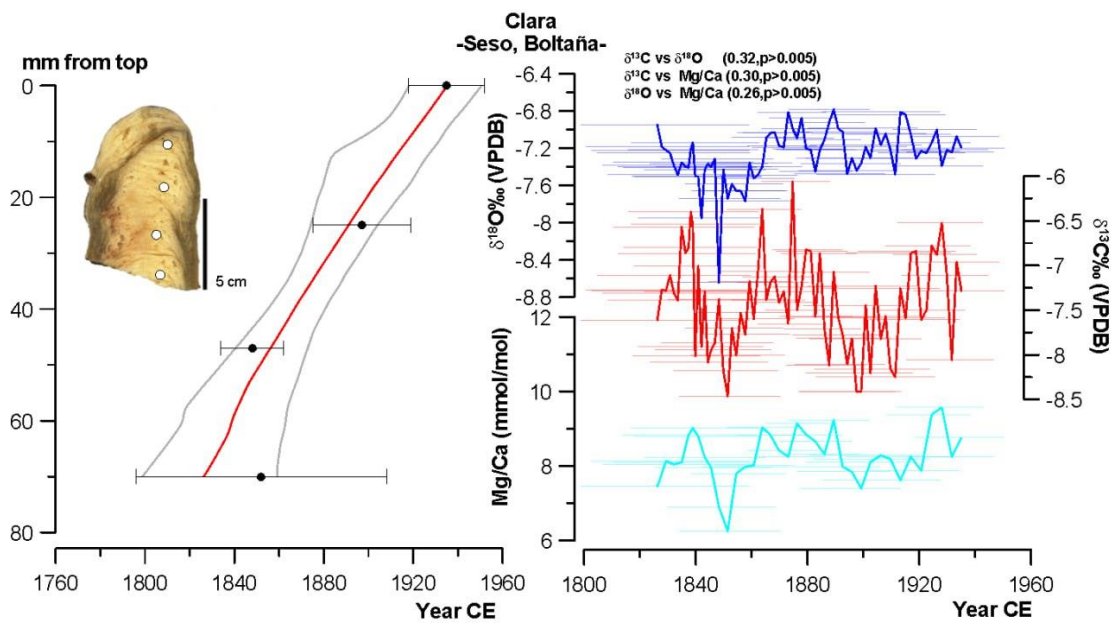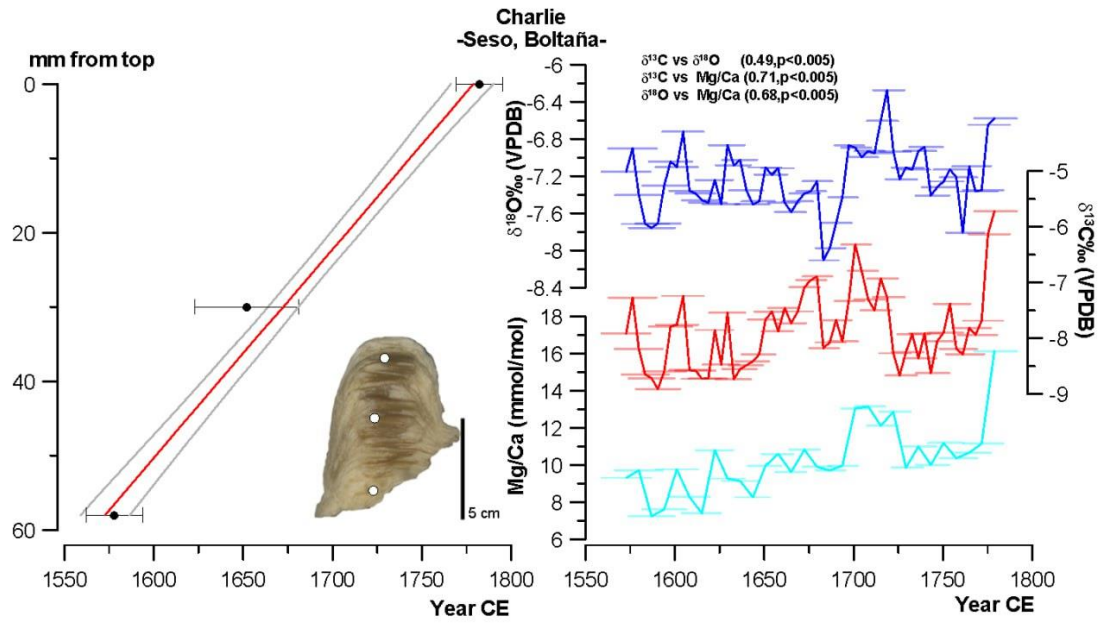
1207

1208

1209

1210

1211

1212

1213

1214

1215

1216   b. Las Gloces cave
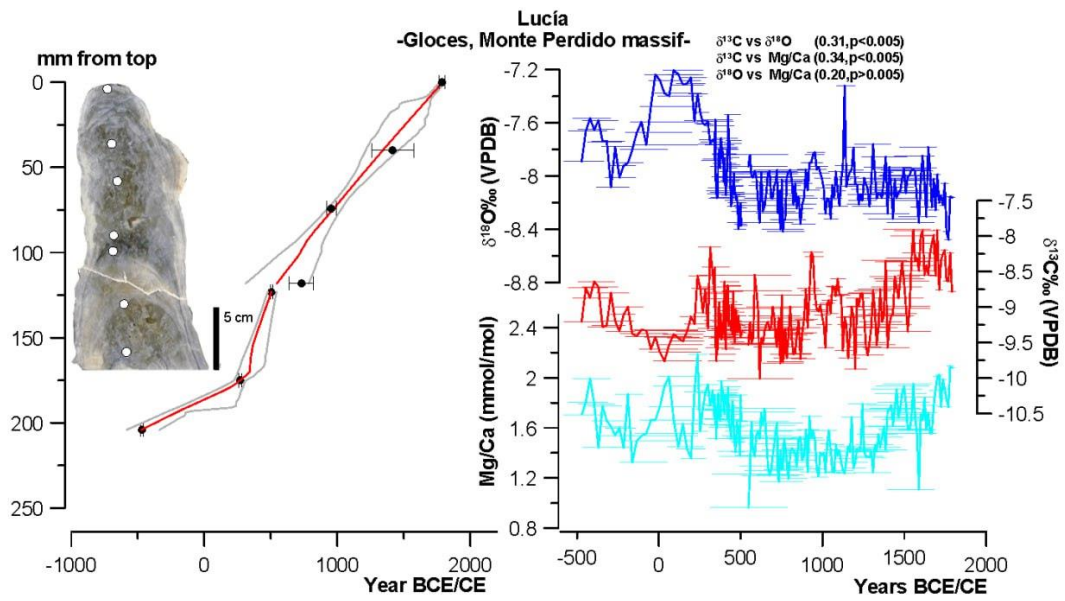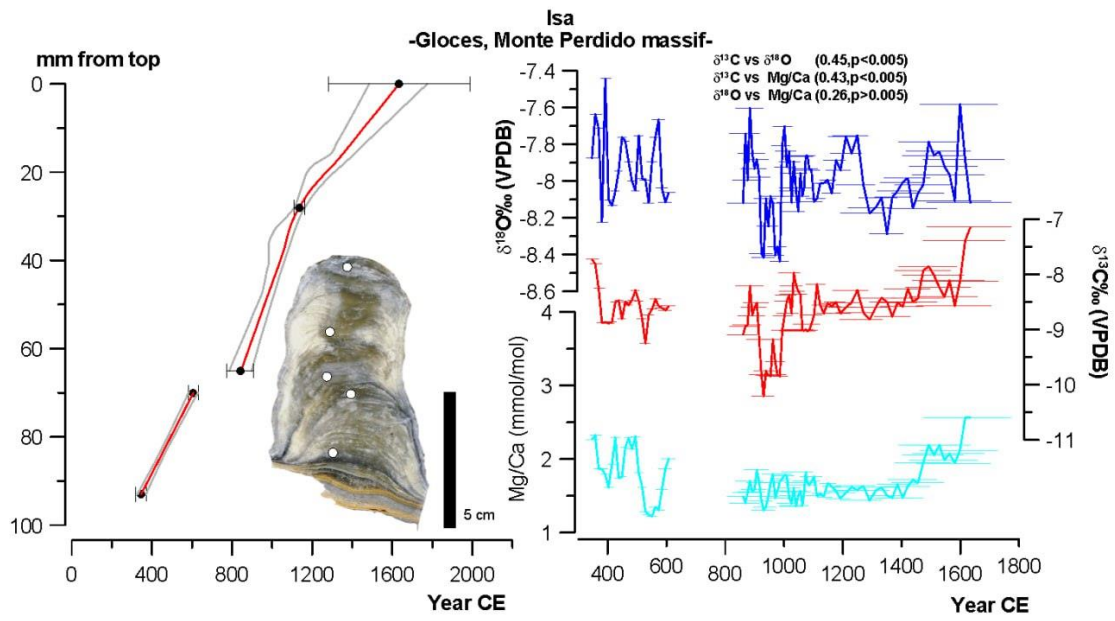
1217

1218

1219

1220

1221

1222

1223

1224

1225   c. B1 cave
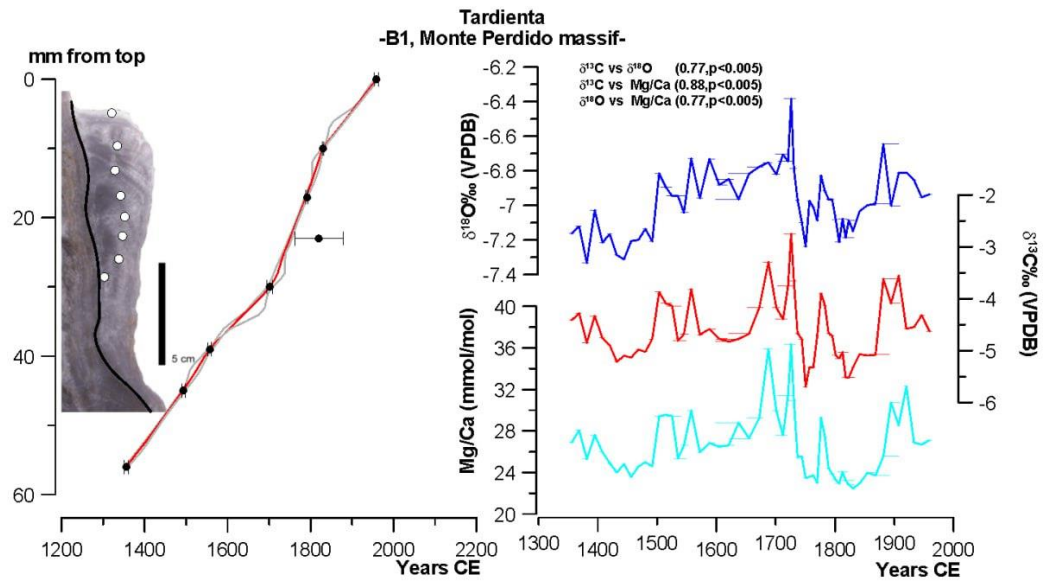
1226   d. Pot au Feu cave
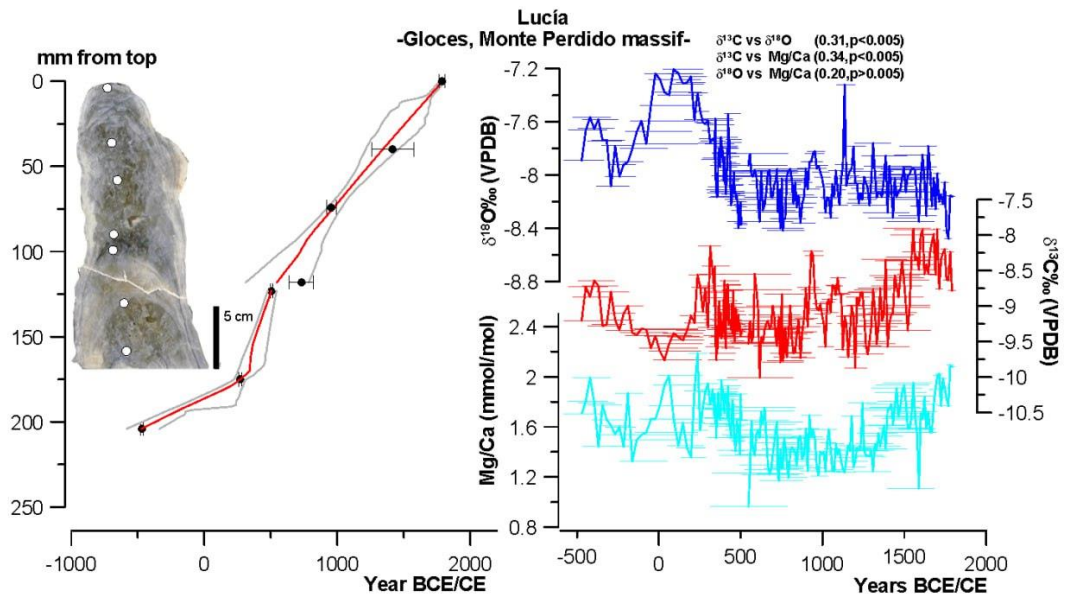
1227

1228

1230 **Figure A2.** Construction of the composite δ¹⁸O record for Seso cave. In the upper graph, the individual
1231 δ¹⁸O profiles of the four Seso stalagmites are presented, using their StalAge models (XEV in red, CHA in
1232 blue, CLA in orange and MIC in green). Some records overlap (mostly between XEV and CHA and XEV
1233 and MIC). The composite δ¹⁸O record for Seso cave is shown in purple on the same y-axis as the individual
1234 curves. The Central Pyrenees δ¹⁸O composite record is shown at the bottom of the graph.

1235
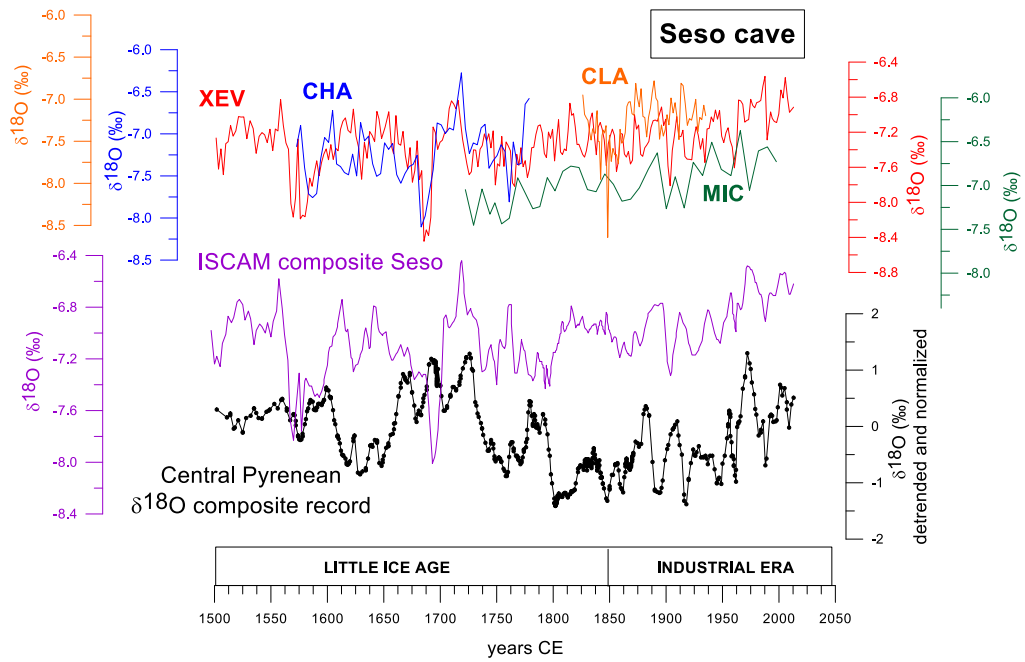
1236

1237

1238 **Figure A3.** Construction of the composite δ18O record for Las Gloces cave. In the upper graph, the δ18O
1239 profiles of the two Las Gloces stalagmites are presented, using their StalAge models (ISA in red and LUC
1240 in blue). The composite δ18O record for this cave is shown in purple curve on the same y-axis as the
1241 individual curves. The Central Pyrenees δ18O composite record is shown at the bottom of the graph. MCA:
1242 Medieval Climate Anomaly, IE: Industrial Era.

1243
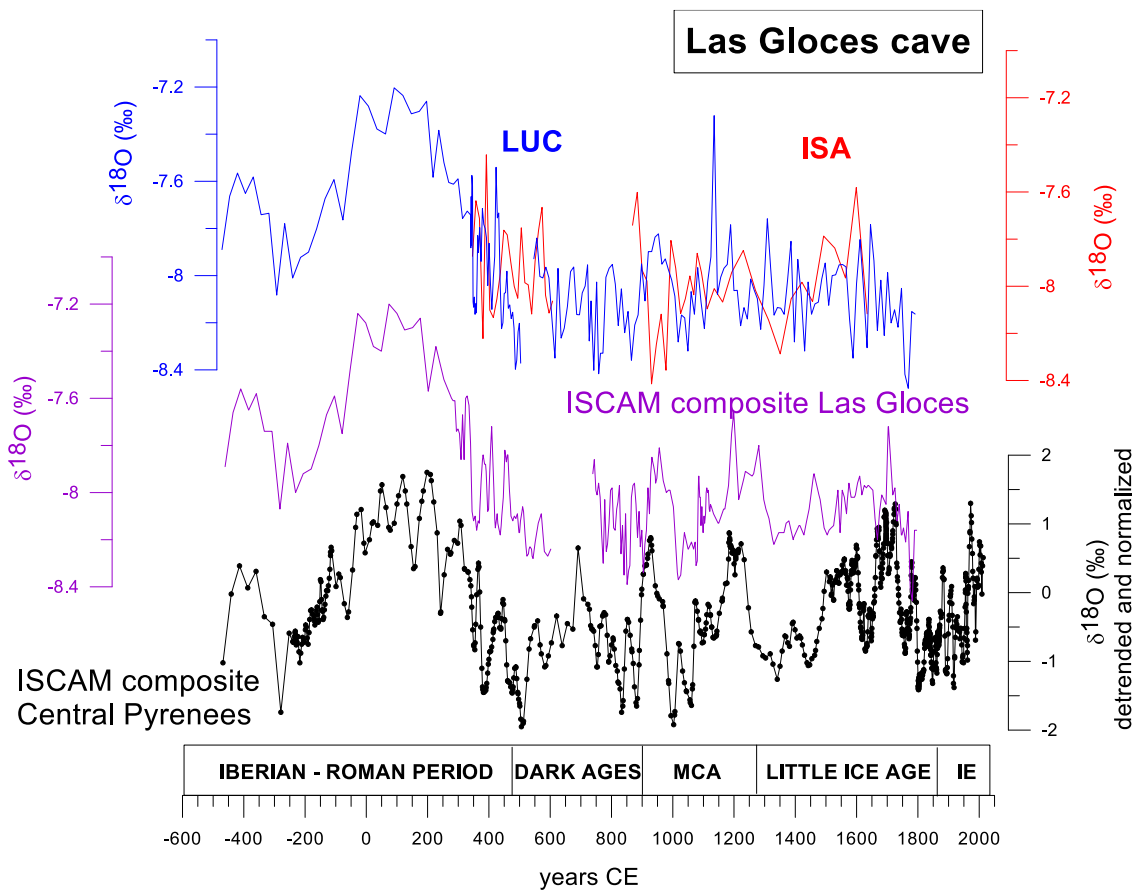
1244
1245
1246

Figure A4. Correlation of (a) composite $\delta^{18}O$ record from MIC and XEV stalagmites with instrumental temperature records at local, regional and global levels. (b) Mean Annual Average Temperature (MAAT) from Goriz hub (AEMET data); (c) MAAT from Pic du Midi de Bigorre (Bücher and Dessens, 1991; Dessens and Bücher, 1995); (d) Minimum Annual Temperature from the Pyrenees from AEMET series (Pérez-Zanón et al., 2017) and (e) MAAT anomalies (respect to 1961-1990 years) using the HadCRUT 5.0.1.0. dataset (Morice et al., 2021). At the bottom, f) $\delta^{18}O$ values of the Pyrenees composite record (in a) compared to North Hemisphere mean annual temperatures (in e) showing a significant correlation.
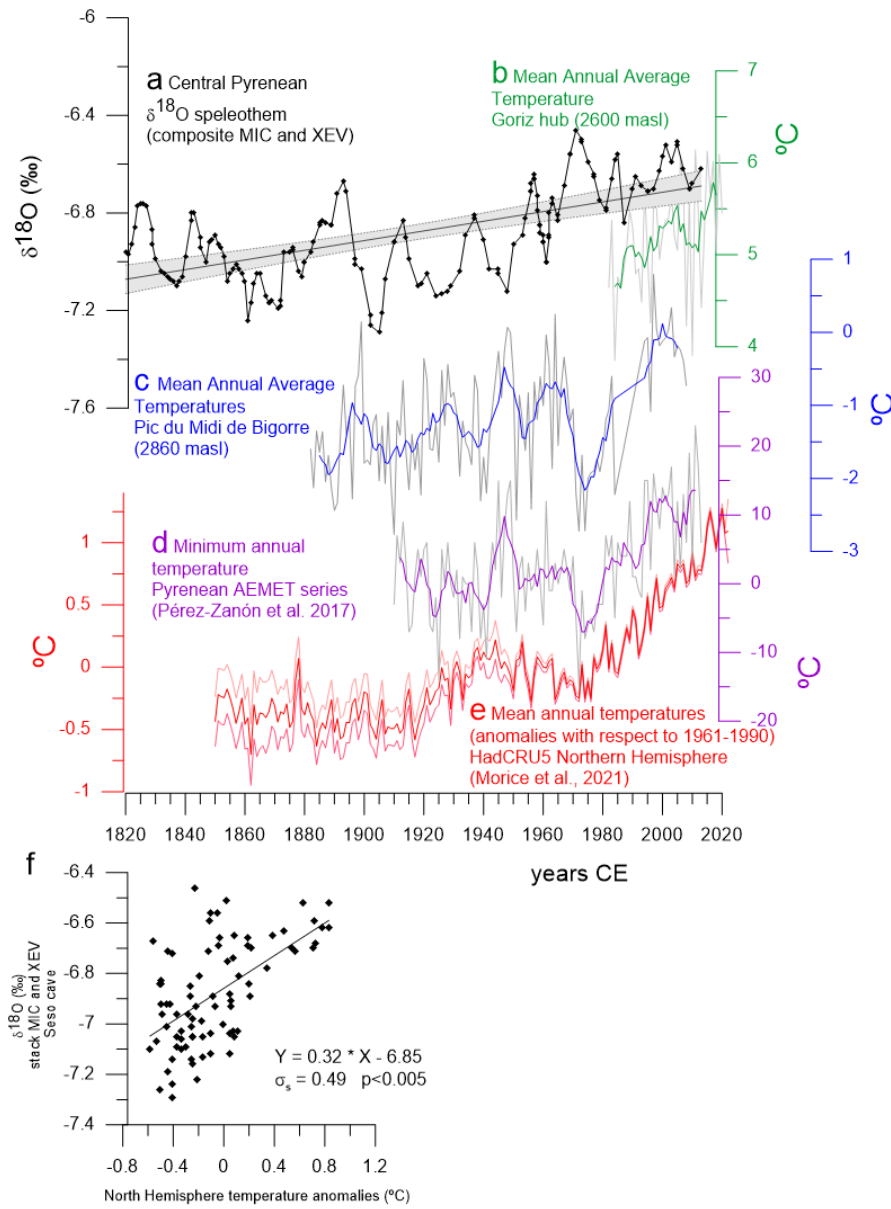
1257 **Figure A5.** Correlation of (a) composite δ^{18}O record from MIC and XEV stalagmites with instrumental
1258 precipitation records at regional levels. (b) Annual precipitation from Goriz hub (AEMET data) and (c)
1259 Precipitation anomalies from the Pyrenees from AEMET series (respect to 1961-1990 years) (Bücher and
1260 Dessens, 1991; Dessens and Bücher, 1995). No significant correlation is observed.

1261

1262

1263